Aalto University
School of Electrical
Engineering

Kimmo Rasilainen

ANTENNA PERFORMANCE IN BENDABLE MOBILE DEVICES

The thesis was submitted in partial fulfilment for the degree of Master of Science in Technology in Espoo, _____.____,2012

Supervisor

Professor Antti Räisänen

Instructor

Lic.Sc. (Tech.) Janne Ilvonen

Aalto University
School of Electrical
Engineering

Abstract

Author:	Kimmo Rasilainen		
Title:	Antenna Performance in Bendable Mobile Devices		
Date:	November 30, 2012	**Number of pages:**	82
Unit:	Department of Radio Science and Engineering		
Field of research:	Radio Engineering		
Supervisor:	Professor Antti Räisänen		
Instructor:	Lic.Sc. (Tech.) Janne Ilvonen		

In this master's thesis, the effect of bending the ground plane of a mobile device on antenna performance is studied using computer simulations and equivalent circuit models. The purpose of the analysis is to identify the changes that can occur when bending the device, and to improve the understanding of the physical reason for these changes.

The results that have been obtained in this work show that when the ground plane of a capacitive coupling element type mobile terminal antenna structure is bent, the characteristic wavemodes of the ground plane experience both resistive and reactive changes, as well as changes in the coupling between the non-radiating antenna element and individual wavemodes.

It is possible to utilise the results of this master's thesis for the design of antenna structures for novel mobile devices with varying degrees of flexibility. In some applications, it may be so that both the ground plane and the antenna element are bendable.

Keywords: bending, effect of the user, equivalent circuit, ground plane wavemodes, quality factor, small antennas

Aalto-yliopisto
Sähkötekniikan korkeakoulu

Tiivistelmä

Tekijä:	Kimmo Rasilainen		
Työn nimi:	Antennin suorituskyky taivutettavissa mobiililaitteissa		
Päivämäärä:	30. marraskuuta 2012	**Sivumäärä:**	82
Yksikkö:	Radiotieteen ja -tekniikan laitos		
Tutkimusala:	Radiotekniikka		
Valvoja:	Professori Antti Räisänen		
Ohjaaja:	TkL Janne Ilvonen		

Tässä diplomityössä tutkitaan, miten mobiililaitteen rungon taivuttaminen vaikuttaa laitteessa käytettävän antennin suorituskykyyn. Analyysin tarkoituksena on tunnistaa erilaiset muutokset, joita taivuttaminen saattaa aiheuttaa antennin toimintaan, sekä lisätä ymmärrystä muutosten fysikaalisista syistä.

Työssä saadut tulokset osoittavat, että taivutettaessa kapasitiivisen kytkentäelementtirakenteen runkoa, rungon ominaisaaltomuodot kokevat resistiivisiä ja reaktiivisia muutoksia sekä muutoksia antennielementin ja ominaisaaltomuotojen välisessä kytkeytymisessä. Kyseisessä antennirakenteessa antennielementti on eisäteilevä.

Diplomityön tuloksia voidaan hyödyntää suunniteltaessa antenniratkaisuja uudenlaisiin taivuteltaviin mobiililaitteisiin. Sovelluksesta riippuen sekä laitteen runko että antennielementti voivat olla taivuteltavissa.

Avainsanat: hyvyysluku, käyttäjän vaikutus, pienet antennit, rungon aaltomuodot, taivutus, vastinpiiri

Preface

This master's thesis is based on research carried out in the RF and Microwave Engineering research group of the Department of Radio Science and Engineering (RAD) in Aalto University School of Electrical Engineering between June and November 2012 under the supervision of Professor Antti Räisänen. I would like to express a few words of gratitude to the people who have contributed to this thesis.

Firstly, I would like to thank Professor Pertti Vainikainen not only for providing me with this highly interesting research topic but also for hiring me as a summer trainee back in 2009. My supervisor, Professor Antti Räisänen deserves thanks for his guidance and and comments that helped to improve the quality of my thesis.

I am deeply grateful to my instructor, Lic.Sc. (Tech.) Janne Ilvonen for his excellent and highly competent guidance during this thesis, and also for the co-operation these past few years. Additionally, Janne's help with LaTeX, both in terms of practical tips as well as the template he kindly provided, is highly appreciated. I am thankful also to Dr. Jari Holopainen and Mr. Risto Valkonen who assisted me with the circuit model used in this work. Also all the other co-workers at the department helped in creating a pleasant working environment.

The antenna group of the RAD department also deserves thanks for providing me with a forum in which to present the progress of my work, especially since my thesis work was not part of any research project. The comments that arose in the discussions greatly benefited the work, and also sparked new ideas for future studies in this field.

Finally, I would like to thank my parents for their support, encouragement and help both during this thesis work as well as throughout my studies.

Helsinki, November 30, 2012,

Kimmo Rasilainen

Contents

List of Abbreviations

C	Capacitor
CAD	Computer Aided Design
CCE	Capacitive Coupling Element
CDMA	Code Division Multiple Access
CTIA	Wireless Association
	(former Cellular Telecommunications Industries Association)
DL	Downlink
DVB-H	Digital Video Broadcasting - Handheld standard
EM	Electromagnetic
FDTD	Finite Difference Time-Domain
FEM	Finite Element Method
FIT	Finite Integration Technique
FM	Frequency Modulation
GPS	Global Positioning System
GSM	Global System for Mobile Communications
IEEE	Institute of Electrical and Electronics Engineers
IFA	Inverted-F Antenna
ILA	Inverted-L Antenna
L	Inductor
LTE	Long Term Evolution
MIMO	Multiple Input Multiple Output
MOM	Method Of Moments
MMD	Mouldable Mobile Device
NFC	Near Field Communication
PEC	Perfect Electric Conductor
PIFA	Planar Inverted-F Antenna
Qi	Standard for wireless charging
R	Resistor
RAD	Radio Science and Engineering (a department in Aalto University)
RF	Radio Frequency

RFID	Radio Frequency Identification
RLC	Resistor Inductor Capacitor
SAM	Specific Anthropomorphic Mannequin
SAR	Specific Absorption Rate
UHF	Ultra High Frequency
UL	Uplink
VNA	Vector Network Analyser
WCDMA	Wideband Code Division Multiple Access
WLAN	Wireless Local Area Network

List of Symbols

BW	bandwidth [Hz]
C	capacitance [F]
C_{ci}	capacitance (ith ground plane wavemode) [F]
$C_{\mathrm{ci,b}}$	capacitance (ith ground plane wavemode) in the bent case [F]
C_{mm}	capacitance (monopole mode) [F]
C_{p}	parasitic capacitance [F]
CF	centre frequency [Hz]
D	largest dimension of an antenna [m]
f_{r}	resonant frequency [Hz]
$f_{\mathrm{r,mm}}$	resonant frequency (monopole mode) [Hz]
I_{eff}	effective electric current [A]
$\jmath$	imaginary unit
k_0	wave number in free space [1/m]
L	inductance [H]
L_{ci}	inductance (ith ground plane wavemode) [H]
$L_{\mathrm{ci,b}}$	inductance (ith ground plane wavemode) in the bent case [H]
L_{mm}	inductance (monopole mode) [H]
n	winding ratio of a transformer
P	power [W]
P_0	power accepted by the antenna [W]
P_{in}	power available at the antenna input [W]
P_{ohmic}	ohmic losses [W]
P_{rad}	radiated power [W]
Q	quality factor
Q_0	unloaded quality factor
$Q_{0,\mathrm{par}}$	unloaded quality factor of a parallel RLC circuit
$Q_{0,\mathrm{ser}}$	unloaded quality factor of a series RLC circuit
Q_{c}	quality factor for conductor losses
Q_{d}	quality factor for dielectric losses
Q_{e}	external quality factor

Q_{el}	quality factor of the antenna element
Q_{gp}	quality factor of the ground plane
Q_{L}	loaded quality factor
Q_{min}	fundamental lowest limit of the quality factor
Q_{mm}	quality factor (monopole mode)
Q_{r}	radiation quality factor
Q_{tot}	total quality factor
Q_{z}	quality factor calculated from input impedance
R	resistance [Ω]
R_{ant}	antenna resistance [Ω]
R_{ci}	resistance (ith ground plane wavemode) [Ω]
$R_{\mathrm{ci,b}}$	resistance (ith ground plane wavemode) in the bent case [Ω]
R_{mm}	resistance (monopole mode) [Ω]
r	radius of a sphere [m]
r_1	boundary between near field and far field [m]
S	scattering parameter
SAR	specific absorption rate [W/kg]
W_{e}	electric energy [J]
W_{m}	magnetic energy [J]
X	reactance [Ω]
X_{ant}	antenna reactance [Ω]
Z	impedance [Ω]
Z_0	characteristic impedance [Ω]
Z_{ant}	complex antenna impedance [Ω]
ϵ_{r}	relative permittivity
η_{m}	matching efficiency
η_{rad}	radiation efficiency
η_{tot}	total efficiency
λ	wavelength [m]
ρ	reflection coefficient
σ	electric conductivity [S/m]
ω	angular frequency [rad/s]

1. Introduction

During the last 20 years, mobile terminals have undergone significant development in terms of size, features as well as number of supported radio systems. In some estimates it has been presented that the number of different antennas within a mobile terminal might even exceed 20 [1]. The different radio systems and their operating bands that the antennas would have to cover are shown in Table 1.1. (The table is gathered based on the specifications of the state-of-the-art Nokia Lumia 920 device [2].) The increasing number of radio systems has also been a driving force for antenna design in mobile terminals, as more and more antennas need to be placed within the limited space of a mobile terminal. With an increasing number of antennas, internal antenna elements have more or less replaced external helical or whip antennas (streamlined mobile terminal instead of a porcupine).

Typical form factors for mobile devices have been candy bar or clamshell type, with possibly some slider functionality implemented. The increasing use of mobile terminals for web browsing and related functionalities has (despite a general desire for more slim-lined and smaller devices) resulted in an increase in overall device and display size. As the mobile devices become ”smarter”, new services and ways of use such as video streaming, navigation, cloud services and other applications have emerged. These applications require data transfer, either over the internet or through a particular radio system. This need for higher data rates can be satisfied by using more antennas and frequencies, or possibly multi-antenna techniques such as MIMO (Multiple Input Multiple Output).

The increased overall volume of the device means that in principle, the space available for a single antenna is larger. However, the increasing number of antennas due to, e.g., MIMO means that the space is also consumed by more antennas. When designing a mobile device, the different antennas should be placed so that they work well enough within the vicinity of not only other antennas but also that of the user. Eventually, as the distance between individual antennas decreases, problems such as poor electromagnetic isolation can be observed.

When a mobile device is in close proximity to the tissues of the user, the performance of the antenna changes from that in free space. Factors such as impedance

Table 1.1. Frequency specifications of some important radio systems used in the Nokia Lumia 920 mobile device [2].

System	UL [MHz]	DL [MHz]	CF [MHz]	Rel. BW [%]
Bluetooth	2400–2483.5	2400–2483.5	2441.75	3.42
GPS	N/A [1]	1575.42	1575.42	0.13
GSM 850	824–849	869–894	859	8.15
GSM 900	880–915	935–960	925	7.61
GSM 1800	1710–1785	1805–1880	1795	7.80
GSM 1900	1850–1910	1930–1990	1920	7.29
LTE 700 (lower)	698–716	728–746	722	6.65
LTE 700 (upper)	777–787	746–756	766.5	5.35
LTE 800	830–840	875–885	857.5	6.41
LTE 850	824–849	869–894	859	8.15
LTE 900	880–915	925–960	925	7.61
LTE 1700	1749.9–1784.9	1844.9–1879.9	1814.9	7.16
LTE 1800	1710–1785	1805–1880	1795	7.80
LTE 1900	1850–1910	1930–1990	1920	7.29
LTE 2100	1920–1980	2110–2170	2045	12.22
LTE 2600	2500–2570	2620–2690	2595	7.32
NFC	13.56[2]	13.56[2]	13.56	0.1
Qi	N/A[3]	N/A[3]	0.2	N/A[3]
WCDMA band V	824–849	869–894	859	8.15
WCDMA band VIII	880–915	925–960	925	7.61
WCDMA band IV	1710–1755	2110–2155	N/A[4]	N/A[4]
WCDMA band II	1850–1910	1930–1990	1920	7.29
WCDMA band I	1920–1980	2110–2170	2045	12.22
WLAN 802.11a	5 GHz band	5 GHz band	N/A[5]	N/A[5]
WLAN 802.11b	2.4 GHz band	2.4 GHz band	N/A[5]	N/A[5]
WLAN 802.11g	2.4 GHz band	2.4 GHz band	N/A[5]	N/A[5]
WLAN 802.11n	2.4/5 GHz bands	2.4/5 GHz bands	N/A[5]	N/A[5]

1) This radio system is intended for reception only.

2) This radio system can be used, e.g., for short range communications with passive tags or between smartphones.

3) Access to information regarding this radio system is limited.

4) Covering the UL and DL bands with a single antenna is impractical due to their large separation.

5) The WLAN bands are separated into several partially overlapping channels with varying bandwidth.

mismatching and absorption of the power into the hand or other body parts can cause significant deterioration in the performance of the antenna [3–8]. These changes in performance should be taken into account during the design process of the antenna, so that the device will still work despite being close to the hand or other parts of the user [9–11]. Wearable GPS antennas are an example of a case in which the antenna structure is bent around the body of the user. Their performance and the changes caused by the presence of the user have been studied in, e.g., [12, 13]. However, wearable antennas have a fundamental difference compared to bendable mobile devices because the antenna can be made larger to overcome the possible detrimental effects of the bending. In mobile devices, this approach may not be suitable because of the limited space.

Even though clamshell-type mobile phones cannot be bent or moulded in an arbitrary fashion, the opening and closing of the cover may have a significant change on the impedance and impedance bandwidth properties of the antenna of a clamshell phone [14, 15]. The antenna has to work reasonably well in both open and closed states, which means that inevitably some compromises have to be made. With bendable or otherwise highly flexible devices, the need for compromises becomes even more apparent as the device should work in a multitude of positions – up to a point in which an intended operating position may not even exist.

Mobile phone manufacturers have proposed different concepts for future flexible or mouldable mobile devices, such as the Morph, Twist and 888 concepts by Nokia [16–18]. In these concepts (illustrated in Fig. 1.1), virtually the whole device can be bent in different ways and into different shapes, thus presenting new challenges for the design. Some commercial designs such as wrist phones have been available, but these (like also the famous 2-way wrist radio of comic figure Dick Tracy) only have a flexible wrist band which does not house the antennas.

a) b) c)

Fig. 1.1. Possible designs for future mobile terminals: a) Nokia Morph, b) Nokia Twist, and c) Nokia 888 concepts [16–18].

Ideas such as the Morph concept are a part of the branch of flexible electronics, which can offer numerous advantages compared to more conventional designs. Therefore, it has been subject of increasing research interest, e.g., [19,20] are both devoted entirely to flexible electronics technology. Flexible designs, such as antennas that can be rolled up when not in use, or RFID (Radio Frequency Identification) tags that conform to the shape of the object it is attached to are examples of future designs enabled by technological advances [21].

For mobile applications, such as mobile phones, increasing device flexibility makes partly or fully flexible displays an interesting future possibility. Depending on the scale of flexibility, different types of displays can be identified. In [22], flexible displays are separated into three categories: curved or conformed, mildly flexible and fully flexible. Fully flexible displays are comparable to paper or cloth, mildly flexible ones do not tolerate, e.g., rolling, and curved ones are not flexed at all during use. The main focus of this thesis is on curved or conformed designs.

In this master's thesis the bending applied to the ground plane is a special case of a concept that could be described with the major term ”mouldable”. This term can be used to describe any modifications that can be performed on the device, including a case of ground plane bending shown in Fig. 1.2. The possible means of changing the shape of the ground plane depend in part on the size and form factor of the device, but they can include, e.g., folding, bending or rolling. Additionally, the concept of Mouldable Mobile Device (MMD) can be used to describe any such devices that can be handled in any of the aforementioned ways.

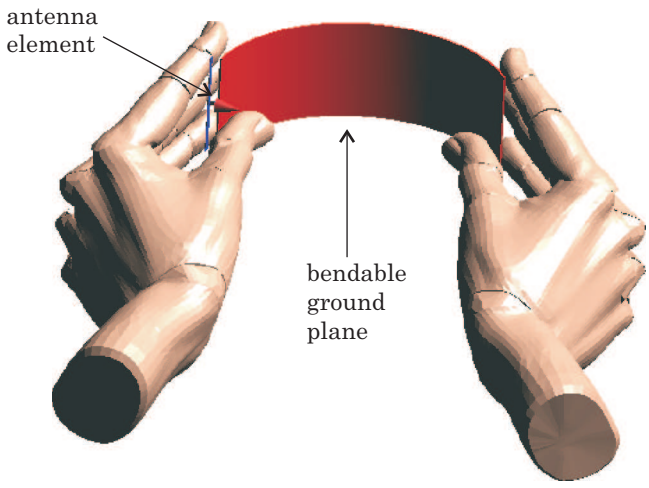

Fig. 1.2. Ground plane bending, one of the possible modifications on the shape of a mobile device. The antenna element is stationary.

The effect of the device bending on the antenna performance is studied in this master's thesis by means of computer simulations, measurements and equivalent circuit

models. In order to see the effects caused by the bending, a couple of simple antenna prototypes were manufactured. These same structures were also studied using commercial EM (electromagnetic) and circuit simulation software to verify the obtained measurement results, but also to determine the suitability of the different computational algorithms (on which the software are based) on the study of conformal designs. One significant aspect of accurate, reliable and (sufficiently) fast simulation software is that they reduce the number of necessary trial-and-error type prototyping rounds considerably. The use of the equivalent circuit model can provide an improved understanding of the physical reasons behind the different effects of the bending.

This thesis is organised as follows. Chapter 2 presents some general theory on mobile terminal antennas, their design and other relevant concepts. The validation process of the different software, the different quantities used to study the performance of the antennas as well as some conceivable problems associated with changing the ground plane shape are discussed in Chapter 3. The performance of the studied mobile terminal antennas in the different use cases, as well as modelling of the bending using a resonator-based equivalent circuit is analysed in Chapter 4. Finally, conclusions are given in Chapter 5.

2. Mobile terminal antennas and effect of the user

This chapter discusses some of the fundamentals of mobile terminal antennas and the effect that the body of the user has on their performance. Antenna properties are discussed in Section 2.1, important quantities and parameters, such as impedance bandwidth and antenna efficiency, are presented in Section 2.2. Section 2.3 explains how mobile terminal antenna structures can be analysed as resonators using an equivalent circuit. Finally, the concept of the user effect is introduced in Section 2.4.

2.1 Fundamentals of antennas

Antennas are devices that are used to transmit and receive radio waves at particular frequencies. Due to their reciprocal nature, the same antennas can be employed both in transmission and reception. However, in some applications it may be necessary to use antennas that are designed only for transmission or reception. These applications include, e.g., FM radio, GPS (Global Positioning System) or DVB-H (Digital Video Broadcasting - Handheld). If an antenna is only receiving, then issues such as signal distortion (caused by, e.g., semiconductors) in the transmitter need not be taken into account.

An antenna radiates an electromagnetic field to its surroundings, and based on its properties, the field can be divided into three separate zones: reactive near field, radiative near field, and far field [23]. In the region closest to the antenna, the reactive near field, the non-radiating field components dominate, there is no distinct radiation pattern, and any obstacles located in the region affect the radiation. Electromagnetic energy (both electric and magnetic) is stored into the reactive near field. In the radiative near field or Fresnel zone, radiating field components dominate and obstacles do not have a clear impact on the radiation. The radiation pattern in the Fresnel zone is still distance-dependent.

When transiting from the Fresnel zone to the far field or Fraunhofer zone, the radiation pattern approaches asymptotically the far-field directional pattern which depends only on direction, not distance. For large antennas, the near field – far field

boundary is at a distance of $r_1 = 2D^2/\lambda$, in which D is the largest dimension of the antenna. In the case of electrically small antennas (such as mobile terminal antennas), the reactive near field boundary is $r = \lambda/2\pi$. This distance is referred to as the radianlength, and it represents the transition between the energy stored in the near field and that radiated in the far field [24]. The exact separation between near field and far field is a bit ambiguous, as the reactive near field of electrically small antennas may extend a few wavelengths from the antenna [23]. An illustration of the radiation regions for an electrically small antenna is given in Fig. 2.1.

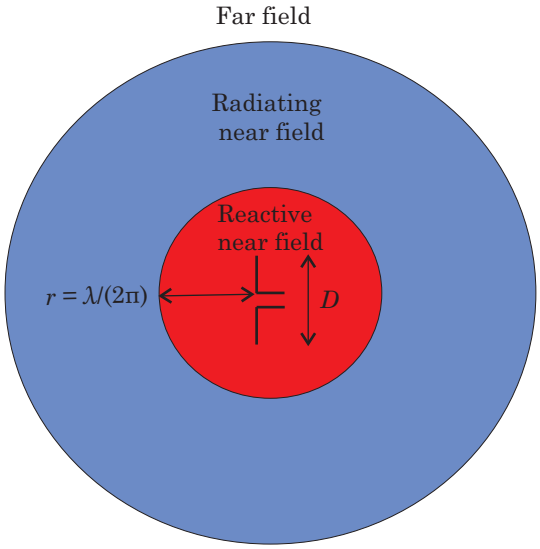

Fig. 2.1. Radiation regions of an electrically small antenna. D is the largest dimension of the antenna and r represents the reactive near field boundary.

2.2 Mobile terminal antennas

The antennas used in current mobile terminals are mainly internal, conformal and electrically small. Conformality means that the shape of the antenna element conforms with the surface of the terminal. An antenna is defined to be electrically small if it can be confined to a sphere whose diameter is small compared to the wavelength at the operating frequency [25]. The radius of the sphere is also the same as the above mentioned far field boundary of electrically small antennas. Among the most important requirements for electrically small antennas are sufficient impedance bandwidth and good enough total efficiency. However, as explained in [26] these requirements are challenging to fulfil simultaneously. Fig. 2.2 illustrates two typical mobile terminal antenna types, the general properties of which are described in the following.

The fundamental property of a small antenna is that it is in resonance at a certain frequency, and the antenna can thus be analysed as a resonator. It is possible to de-

sign two distinct types of small antennas: resonant type structures and non-resonant type structures that are either self-resonant or non-self-resonant. When an antenna is of the resonant type, a particular operating frequency is achieved by optimising the geometry, and the volume occupied by the antenna is used to create the resonance. An example of resonant type antennas is the Planar Inverted-F Antenna or PIFA (see Fig. 2.2a), which has been often used in mobile terminals. Other examples include Inverted-F Antennas (IFA) and Inverted-L Antennas (ILA). In order to achieve a good radiation performance, self-resonant antennas should have dimensions on the order of $\lambda/4$. Particularly at lower frequencies where the wavelength is longer, this requirement becomes challenging due to the limited volume available within the mobile terminal.

One solution to overcome the size issue is to use non-resonant type antenna elements (see Fig. 2.2b), which have been introduced in [27]. In these, the operating frequency is not determined by the geometry of the antenna element, but instead an external matching circuit is used to generate the resonance. A more detailed discussion on the mechanism behind obtaining the resonance will be provided later, but in essence it is a question of countering the excess amount of capacitive (electric) or inductive (magnetic) energy stored in the near field of the antenna with a circuit element of opposite type. With a suitable matching circuit (see Fig. 2.2b) it is possible in theory to match the antenna to any frequency. Capacitive Coupling Elements (CCEs) are an example of non-self-resonant antenna elements that are mainly used to couple to the currents of the ground plane wavemodes [27]. Even though the size of non-resonant type antennas can be made smaller than their resonant-type counterparts, it is worth keeping in mind that the size cannot be arbitrarily reduced without decreasing the performance of the antenna [26].

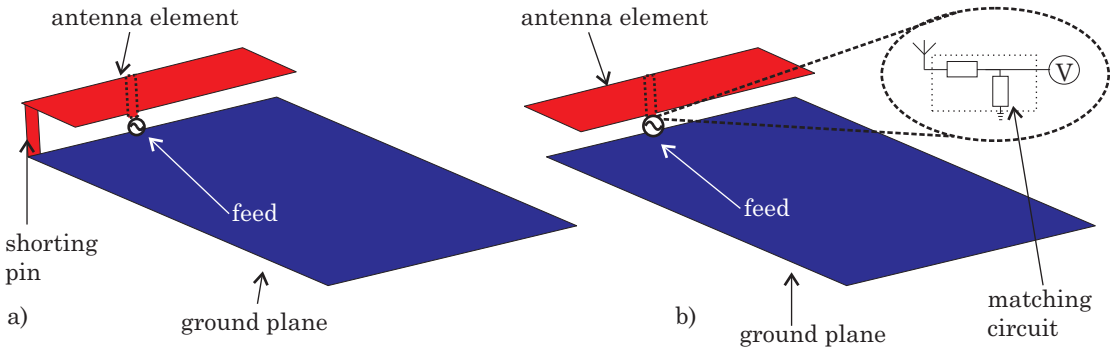

Fig. 2.2. Schematic illustrations of a) PIFA and b) CCE antennas.

2.2.1 Antenna impedance and impedance matching

In mobile devices, as in many other RF (radio frequency) and microwave applications, good matching between the antenna and the feeding network is important. Due to the limited battery capacity of the mobile devices, the importance of the matching further increases, as power lost due to the improper matching may considerably reduce the operating time of the device. Mobile terminal antennas are not standalone devices, but they are part of the transceiver. Other parts of RF electronics, such as input or output stage amplifiers, may require a particular impedance value or matching level in order to operate efficiently [28].

The load impedance of an electrically small antenna consists of a resistive (real) and reactive (imaginary) part

$$Z_{\mathrm{ant}} = R_{\mathrm{ant}} + \jmath X_{\mathrm{ant}}, \tag{2.1}$$

in which the resistive part can be divided into radiation resistance (R_{r}) and loss resistance (R_{L}). The loss resistance takes into account the losses in the antenna structure. The radiation resistance is coupled from free space to the terminal of the antenna, and it does not represent any actual resistance of the antenna (the antenna is seen by the transmission lines to which it is connected as a resistance) [29]. The reactive part, which is caused by energy stored in the near field of the antenna, may be separated into capacitive and inductive part, so that Eq. (2.1) can be re-written as

$$Z_{\mathrm{ant}} = R_{\mathrm{r}} + R_{\mathrm{L}} + \jmath\omega L + \frac{1}{\jmath\omega C} = R_{\mathrm{r}} + R_{\mathrm{L}} + \jmath\left(\omega L - \frac{1}{\omega C}\right), \tag{2.2}$$

in which L and C are the inductance and capacitance, respectively, and $\omega = 2\pi f_{\mathrm{r}}$ is the angular resonant frequency.

In practice, the impedance of the antenna differs from the characteristic impedance (Z_0) of the transmission line feeding the antenna. In this case, a part of the transmitted power is reflected back from the antenna. The reflection coefficient (ρ) is a measure of how well the transmission line and the antenna are matched together. It can be expressed with the help of the antenna impedance and the characteristic impedance as

$$\rho = \frac{Z_{\mathrm{ant}} - Z_0}{Z_{\mathrm{ant}} + Z_0}. \tag{2.3}$$

If the reflection coefficient is zero, then the antenna is perfectly matched to the transmission line. In order to reduce the reflections, particularly with non-resonant antennas, an external matching circuit can be employed. It is possible to use either single or multi-resonant matching, depending on the needs of a particular application.

Multi-resonant matching requires the use of several resonators, and the impedance bandwidth that can be obtained with the matching circuit initially increases with the number of resonators. However, as discussed in [30], the benefit obtained from additional resonators saturates quite fast, and five resonators already provides 90 % of the maximum available bandwidth. In practice, matching network complexity, resonator losses and similar factors limit the feasible number of resonators to two or three.

It is possible to implement the matching circuit using either distributed or lumped elements, depending on the target frequency. At lower frequencies, the size of distributed elements such as stubs implemented with microstrip lines become impractically large. Lumped elements, such as resistors (R), inductors (L) and capacitors (C), on the other hand, are suitable at frequencies up to around 2-3 GHz. At higher frequencies the size of the element begins to approach one wavelength, hence making the assumption of lumped elements no longer valid. All lumped elements (R, L or C) have some losses (resistance) that increase as the frequency goes higher. Additionally, the fundamental functionality of the element may change, meaning that beyond some particular frequency, a capacitor might begin to act as an inductor, for instance.

If the real part of the impedance to be matched is not zero, it is possible to perform the matching by using a two-element reactive matching circuit (inductors and capacitors). Depending on the location of the normalised impedance on the Smith chart, it can be shown that there are two or four possible matching circuit topologies, as explained, e.g., in [31]. The different topologies that can be applied within the different regions are depicted in Fig. 2.3.

2.2.2 Impedance bandwidth and quality factor

An important parameter describing the performance of the antenna is the (relative) impedance bandwidth. It presents the frequency range within which a certain antenna parameter (such as matching level), is better than some specified value. A typical matching criterion used for determining the impedance bandwidth of an antenna is, e.g., –6 dB. The relative bandwidth is obtained when the bandwidth is given with respect to the centre (or operating) frequency. For electrically small antennas, the bandwidth can be calculated with the help of the unloaded quality factor (Q_0) and a specified matching criterion (S) at the band edge as

$$BW = \frac{S-1}{Q_0\sqrt{S}}. \tag{2.4}$$

It is sometimes useful to compare the bandwidth obtained with a particular match-

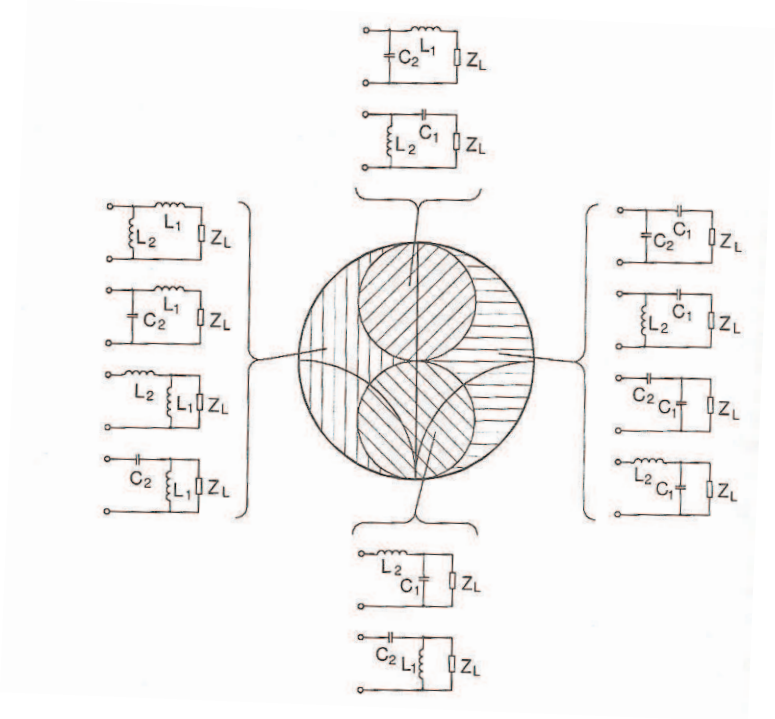

Fig. 2.3. Possible two-element matching circuit topologies (picture taken from [31]).

ing circuit to that which would be available theoretically. The maximum available bandwidth for an unmatched load is given by the Bode-Fano criterion, in which the load impedance is matched using an infinite number of ideal lumped matching components [34, 35]. This bandwidth cannot be reached in practice, but it provides a theoretical estimate of the quality of the matching. One corollary of the Bode-Fano criterion is that the perfect matching (meaning zero reflection) can only be obtained at single frequencies, not over a certain frequency band.

The ability of a resonator to store electromagnetic energy is taken into account with the quality factor (Q), which is the other feature of the resonance phenomenon besides the resonant frequency [36]. It is also a measure of the losses in different parts of the resonator circuit [31], and it is defined as

$$Q = \frac{\omega_{\mathrm{r}} W}{P_{\mathrm{L}}}, \tag{2.5}$$

in which $\omega_{\mathrm{r}} = 2\pi f_{\mathrm{r}}$ is the angular resonant frequency, W is the energy stored in the resonator and P_{L} is the loss power. Because mobile terminal antennas are electrically small, they can be analysed using resonator-based models (including the Q).

The electromagnetic energy stored in the near field of the antenna consists of electric or capacitive energy (W_{e}) and magnetic or inductive energy (W_{m}). Additionally, the loss power can be divided into radiation losses (P_{rad}) and ohmic losses (P_{ohmic}), of which the latter is zero for lossless antennas. The Q of Eq. (2.5) can hence be

expressed as [37]

$$Q = \frac{\omega_{\mathrm{r}}(W_{\mathrm{e}} + W_{\mathrm{m}})}{(P_{\mathrm{rad}} + P_{\mathrm{ohmic}})}. \tag{2.6}$$

The electric and magnetic energies of the previous expression are also connected to the reactive part of the antenna impedance given in Eq. (2.2). As presented in [37], the reactance for an input-current defined system can be expressed as

$$X = \frac{2(W_{\mathrm{m}} - W_{\mathrm{e}})}{|I_{\mathrm{eff}}|^2}. \tag{2.7}$$

At the resonance, the reactance is zero (meaning $W_{\mathrm{e}} = W_{\mathrm{m}}$), so that Eq. (2.6) can be re-written as

$$Q = \frac{2\omega W}{P}. \tag{2.8}$$

If the electric and magnetic energies stored are not the same (particularly for non-resonant type antennas), the impedance of the antenna is either capacitive or inductive – depending on which of the energies is larger. As an example, the impedance of a capacitive coupling element is capacitive (as one might expect from the name). This means that a suitable inductive circuit element is to be added to the structure in order to balance the energies and thereby obtain the desired resonance.

For electrically small unmatched antennas, it is possible to determine the Q calculated from the unmatched impedance data by using the approximate formula [38]

$$Q_{\mathrm{z}} = \frac{\omega_0}{2R_0\omega_0}|Z_0'(\omega_0)| = \frac{\omega_{\mathrm{r}}}{2R(\omega_{\mathrm{r}})}\sqrt{[R'(\omega_{\mathrm{r}})]^2 + \left[X'(\omega_{\mathrm{r}}) + \frac{|X(\omega_{\mathrm{r}})|}{\omega_{\mathrm{r}}}\right]^2}, \tag{2.9}$$

in which $R(\omega_{\mathrm{r}})$ and $X(\omega_{\mathrm{r}})$ are the input resistance and reactance, respectively, of the antenna at the resonant angular frequency. The corresponding quantities marked with primes are the respective frequency derivatives. This formula is also known as the Yaghjian-Best formula (after the authors of [38]).

The impedance bandwidth is inversely proportional to the Q. However, even though a smaller Q indicates wider bandwidth, the Q has a fundamental lower limit (known as the so-called Chu-Harrington limit) [26, 39, 40]

$$Q_{min} = \frac{1}{k_0 r} + \frac{1}{(k_0 r)^3}, \tag{2.10}$$

in which k_0 is the wave number in free space and r is the radius of the radiansphere within which the antenna is enclosed and within which it stores no energy. The Chu-Harrington limit can be used to estimate the maximum available bandwidth for a particular size of the antenna. However, it cannot be reached with any realisable antennas.

The unloaded quality factor Q_0 is a measure of the losses of the resonator itself. These include conductor, dielectric and radiation losses (Q_{c}, Q_{d} and Q_{r}, respectively).

The losses outside the resonator can be expressed with the help of the external quality factor Q_e. The loaded quality factor Q_L takes into account the losses of the entire circuit, and it can be expressed with the help of the unloaded and external quality factors as follows

$$\frac{1}{Q_\mathrm{L}} = \frac{1}{Q_0} + \frac{1}{Q_\mathrm{e}} = \frac{1}{Q_\mathrm{r}} + \frac{1}{Q_\mathrm{c}} + \frac{1}{Q_\mathrm{d}} + \frac{1}{Q_\mathrm{e}}. \tag{2.11}$$

If the resonator losses are larger than the external losses ($Q_\mathrm{e} > Q_0$), the antenna is said to be undercoupled. If external losses are larger ($Q_\mathrm{e} < Q_0$), the antenna is overcoupled. In the case where the losses are equal ($Q_\mathrm{e} = Q_0$), the antenna is critically coupled at the resonant frequency. When designing mobile terminal antennas, some overcoupling is generally desired as it has been shown that the bandwidth can be maximised by using optimal overcoupling [32]. Additionally, an overcoupled antenna is better with respect to the user effect, because the losses introduced by the user reduce the size of the loop, thereby decreasing the coupling and improving the obtained matching. This effect has been discussed, e.g., in [41].

Even though the resonant frequency of the antenna can be observed in the Cartesian reflection coefficient curve ($|S_{11}|$), this plot does not provide complete information of the matching. In order to see the coupling, the full S_{11} parameter should be viewed on the Smith chart. An example of the different coupling cases for a simple CCE structure is shown in Fig. 2.4.

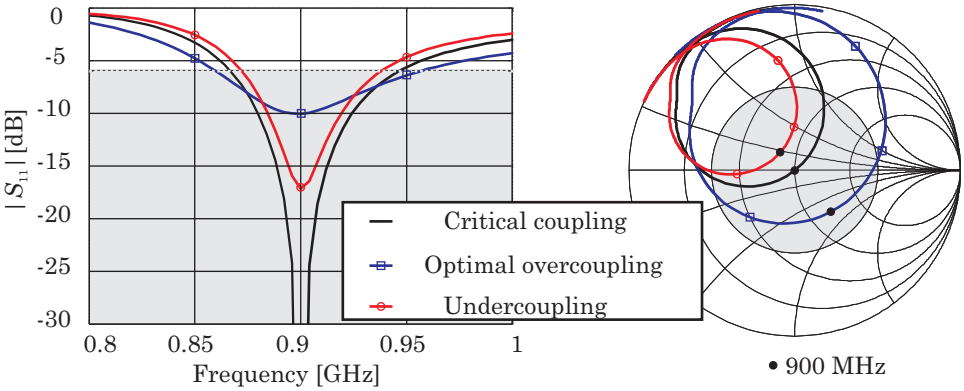

Fig. 2.4. Example of critical, over-, and undercoupling for a CCE antenna structure. The grey area indicates the region where the matching level is –6 dB or better.

The antenna is matched using a two-element matching circuit. As can be seen from the Cartesian reflection coefficient curves, the broadest impedance bandwidth is achieved when the antenna is optimally overcoupled. The effect of coupling on the bandwidth has been discussed, e.g., in [32].

2.2.3 Bandwidth potential

One useful quantity that can be used to study the impedance behaviour of mobile terminal and other antenna systems is bandwidth potential. This concept was first introduced in [27], and it provides a fair means of comparing two different antenna structures. The bandwidth potential describes the bandwidth that can be obtained with a particular antenna using a two-element matching circuit in such a way that the antenna fulfils the desired matching criterion at each frequency [33].

The main benefit of the bandwidth potential is that it enables a quick comparison of the bandwidth that can be obtained with a particular antenna without having to tune the antenna to resonate at a given frequency. It works best when the reflection coefficient is not too large, i.e. when the impedance is not too close to the edge of the Smith chart [33]. This is due to the fact that the larger the reflection coefficient is, the faster the impedance seen through the matching circuit will vary, and correspondingly the resonance that is obtained will be highly narrowband.

2.2.4 Antenna efficiency

Antenna efficiency is an important concept that describes how the antenna is able to convert the input power into radiation (in transmission) or how it converts received radiation to, e.g., voltage (in reception) Efficiency is closely connected to the quality of the matching described earlier. By definition of the IEEE, radiation efficiency (η_{rad}) describes the ratio of the power radiated (P_{rad}) by the antenna to the net power accepted by the antenna (P_0) [25]

$$\eta_{\mathrm{rad}} = \frac{P_{\mathrm{rad}}}{P_0}. \tag{2.12}$$

For electrically small antennas, the radiation efficiency can also be expressed with the help of radiation and loss resistances (R_{r} and R_{L}, respectively) as follows

$$\eta_{\mathrm{rad}} = \frac{R_{\mathrm{r}}}{R_{\mathrm{r}} + R_{\mathrm{L}}}. \tag{2.13}$$

Antenna matching is taken into account by the matching efficiency, which is defined as the ratio of the power accepted by the antenna to the total power available at the antenna input

$$\eta_{\mathrm{m}} = \frac{P_0}{P_{\mathrm{in}}}. \tag{2.14}$$

A quantity that takes into account both the matching and radiation efficiency is the total efficiency, which is defined as the product of the two efficiencies

$$\eta_{\mathrm{tot}} = \eta_{\mathrm{rad}}\eta_{\mathrm{m}}. \tag{2.15}$$

In the case of one-port structures, such as antennas, it is possible to determine η_{m} also based on the reflection coefficient. With only one port, the reflection coefficient is commonly referred to as $\rho = S_{11}$, which is one of the so-called scattering or S parameters commonly used in microwave engineering. The connection between the matching efficiency and the reflection coefficient is

$$\eta_{\mathrm{m}} = 1 - |S_{11}|^2. \tag{2.16}$$

This relation is meaningful for both simulations and measurements. In the simulations, one may obtain the η_{tot} of a non-resonant type antenna by performing the EM simulation for the unmatched case (yielding η_{rad}) and matching the antenna with a circuit simulator (giving η_{m}). Somewhat depending on the properties of a particular antenna measurement system, one may obtain at least the input impedance and η_{tot} of an antenna structure. These quantities can then be used to determine the η_{rad}, as has been performed in [42] for both in free space and in the presence of the user.

2.3 Mobile terminal antenna as a resonator

In mobile terminals, properties such as impedance bandwidth are determined by the behaviour of both the antenna and the ground plane. As presented in [43], the performance of mobile terminals and other small radio devices (whose dimensions are smaller than one wavelength) can be studied as the combination of separate antenna element and ground plane wavemodes. An equivalent circuit, in which the antenna element and ground plane are modelled as resonators, can be derived for the structure. The characteristic wavemodes of the ground plane provide an insight into its radiation properties.

2.3.1 Resonator-based equivalent circuit

The input impedance of the combined antenna element and ground plane structure can be modelled using an equivalent circuit, an example of which is illustrated in Fig. 2.5 [44]. The circuit of Fig. 2.5 describes the behaviour of the so-called monopole mode and k number of ground plane wavemodes (meaning k resonant frequencies) of a CCE antenna structure. In the circuit, the parallel RLC resonators represent the ground plane wavemodes, and the series RLC resonator models the antenna (monopole mode). The name monopole refers to the fact that the impedance behaviour of the CCE resembles that of a top-loaded monopole placed on a ground plane at UHF (Ultra High Frequency), as discussed in, e.g., [45]. As is explained in [43],

the circuit model approach can be generalised to any antenna, provided that relevant parameters for the element are known (particularly its radiation quality factor).

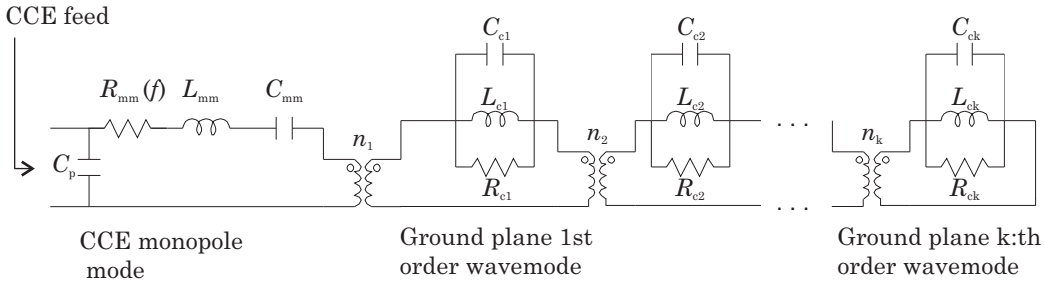

Fig. 2.5. Equivalent circuit for the ground plane and antenna of a mobile terminal (picture modified from [44]).

With a larger number of resonators, the accuracy and the frequency range at which the model is valid increases, but so does also the complexity of the circuit. One of the advantages of the circuit models is that they may provide a more profound understanding of the physics behind particular antenna behaviours (the components represent actual physical quantities). A circuit synthesis based approach for modelling the input impedance of a coupling element is also possible, but this approach would mostly lose the physics behind the phenomena [44].

The element values for the components of the equivalent circuit can be determined based on the Q and resonant frequency of particular wavemodes. The Q_0 of series and parallel RLC resonator circuits can be expressed as [46]

$$Q_{0,\mathrm{ser}} = \frac{\omega_0 L}{R} = \frac{1}{\omega_0 RC} \tag{2.17}$$

for the series resonator, and correspondingly for the parallel resonator

$$Q_{0,\mathrm{par}} = \omega_0 RC = \frac{R}{\omega_0 L}. \tag{2.18}$$

The equivalent circuit model and its individual resonators partly help to explain why the overall quality factor (Q_{tot})of the antenna structure has contribution from both the antenna element (Q_{el}) and the ground plane (Q_{gp}).

In the monopole mode (series RLC resonator in Fig. 2.5), the value of the resistor is frequency-dependent, and its value is given as [44]

$$R_{\mathrm{mm}}(f) = R_0 \left(\frac{f}{f_{\mathrm{r,mm}}} \right)^2, \tag{2.19}$$

in which R_0 is the input resistance of the monopole mode at the resonant frequency of this wavemode ($f_{\mathrm{r,mm}}$). The parasitic capacitance C_{p} shown in the circuit of Fig. 2.5 satisfies the requirement of zero impedance at the feed of the coupling element at infinite frequency [44].

Conventionally, the Q_0 of the antenna element is determined by placing the element on top of a very large ground plane (ideally an infinite ground plane), as discussed, e.g., in [47]. Another method was suggested in [44], in which it is possible to determine the Q of the monopole mode by finding the maximum Q_0 through different ground plane lengths (when the antenna element is positioned at the centre of the ground plane). In this case, the width of the ground plane has correct dimensions. With the ground plane length giving the maximum Q_0, also referred to as the Q_{mm}, the radiation is (ideally) due to the antenna element alone, meaning that the ground plane does not radiate. Once the correct dimensions have been found, the frequency at which the reactance of this structure is zero is $f_{\mathrm{r,mm}}$, and the value of the resistance at this frequency gives the $R_{\mathrm{mm}}(f_{\mathrm{mm}})$.

When studying the Q of the ground plane wavemodes, it is important to notice that, e.g., the calculated Q_{z} takes into account the entire antenna structure, meaning both the antenna element and the ground plane. For the ground plane wavemodes, their Q can be calculated numerically using the so-called characteristic wavemode theory which is discussed more in Section 2.3.2. An example of this kind of analysis can be found, e.g., in [48], in which the radiation quality factor (Q_{r}) of the first few resonant wavemodes of a mobile terminal ground plane are studied using a plane wave excitation (no antenna element or feed).

It is also possible to take into account the effect of the body of the user in the equivalent circuit-based model with suitable additional parasitic components. The parasitic components cause a change in the resonant frequency and quality factor (separate components are needed for each wavemode), and they model the lossy dielectric material that is placed in the near fields of the wavemodes [49]. By suitably modifying the equivalent circuit, it is also possible to consider the effect of ground plane bending on antenna performance. The exact number and type of the additional components required will become more clear once the effect of the ground plane bending has been observed. This subject will be discussed further in Section 4.5.

2.3.2 Characteristic wavemodes of the ground plane

As the combination of the antenna and the ground plane of a mobile terminal can be modelled using a resonator-based model, it is possible to determine the characteristic wavemodes of the ground plane. The shape of the ground plane is most often rectangular, but it has been shown in [50] that it is possible to determine characteristic modes for conducting bodies of arbitrary shape. Mathematically speaking, determining the characteristic wavemodes means solving a particular eigenmode prob-

lem [51]. Illustrations of some of the shapes of the wavemodes that can be formed on the ground plane are given, e.g., in [52, 53].

When comparing the wavemodes of a real antenna structure (both ground plane and element) to the illustrations given in the aforementioned articles, some differences are to be expected, as the illustrations in the articles are for the case without any antenna element. The first five radiating modes that can be found in a conducting ground plane are shown in Fig. 2.6. Of the different current modes of Fig. 2.6, Types 1 and 4 are most commonly used with patch-type antenna structures [53].

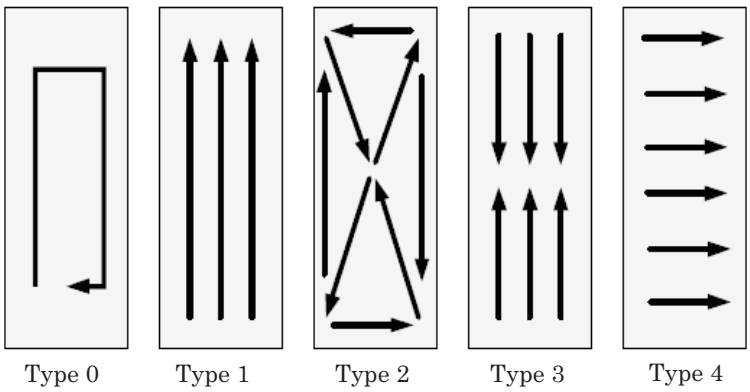

Fig. 2.6. Current modes of a conducting ground plane (picture from [52]). The arrows indicate the directions in which the currents are flowing in a particular mode.

These wavemodes can be of either resonant or non-resonant type, and they are characterised by their surface current distributions. The resonant wavemodes (also referred to as ”ground plane resonances”) are those that contribute to the radiation of the ground plane, whereas non-resonant modes often have poor radiation properties. The contribution of the ground plane wavemodes to the overall radiation of the mobile terminal is important especially at lower frequencies: at, e.g., 900 MHz, the radiation losses of the antenna element is typically only about 10 % of the total power, while the rest is due to the ground plane [43]. The fact that the ground plane is the main radiator at lower frequencies is one of the reasons why self-resonant antennas such as PIFAs can be replaced by simpler, non-radiating coupling elements.

When bending the ground plane, the different wavemodes may be affected in different ways. The behaviour depends most likely on both the direction and shape of the surface current at a particular wavemode as well as on the direction along which the ground plane is bent (along major or minor axis, or a suitable combination of these).

2.4 Effect of the user

As is well-known, the presence of the user in realistic use cases changes the performance of the antenna compared to free space conditions. These changes include impedance mismatching, changes in efficiency (both radiation and matching efficiency), as well as in the radiation pattern of the antenna. Most of these changes are detrimental for the operation of the antenna, but also some positive effects have been reported [54, 55]. In addition to the effect that the user has on the antenna, the antenna may also affect the user, e.g., by means of power absorption into the tissues [56].

Mobile devices are seldom used in free space like conditions, making it important to take into account also the effect of the user in the antenna design. Internal antennas that are very common in today's devices are often more sensitive to the effect of the user than external ones [57]. One of the reasons behind this effect is that it is trivial to avoid touching an external antenna, whereas the exact locations of internal elements – and thereby the most suitable hand grip – is considerably more challenging to determine. In general, there are differences in preferred hand grips and slight anatomical variation between users. This indicates that the effect of the user should be studied by means of statistical analysis. Statistical studies on the effect of the user have been performed in, e.g., [58, 59].

When a mobile terminal is operated in a realistic use case, parts of the body are inevitably located in the near field of the antenna, causing part of the transmitted power to be absorbed into the tissues. This power is then ”lost” from data transmission point-of-view. An example of the absorption of power into the hand is shown in Fig. 2.7, from which one can see that the absorption is not constant but it is different both for different parts of the hand and for different frequencies. When considering traditional mobile terminals in talk or data modes, in particular the power absorbed into the head and hand is studied. The power absorbed heats the tissues, and this is one of the biological effects of radio waves that has been demonstrated [60]. A measure of the power absorbed in the tissues is *SAR* (Specific Absorption Rate), and limits that all devices have to fulfil in order to get a sales permit have been defined. Knowing the *SAR* value of the mobile device is especially important in the talk mode, and for this reason this quantity is omitted from this work.

In addition to power absorption, the presence of human tissue changes the input impedance of the antenna, which can have a considerable effect on matching. Changes in the impedance caused by the dielectric loading also shifts the resonant frequency from the free space case. Due to the shift in resonant frequency, the match-

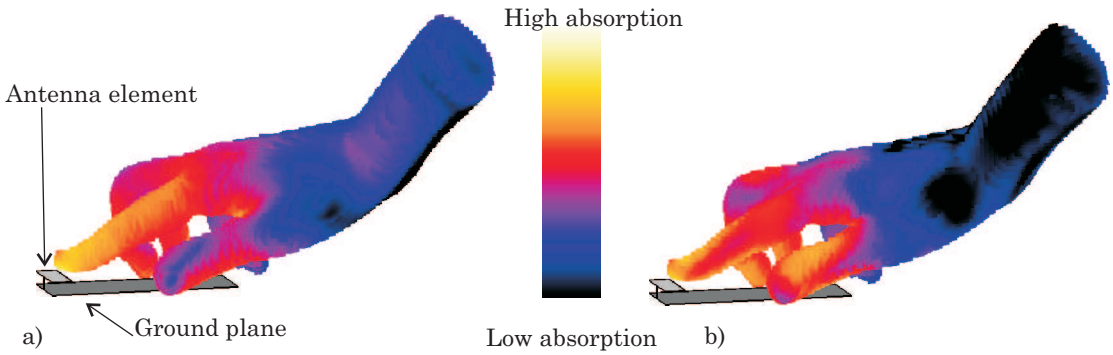

Fig. 2.7. Example of power absorption into the hand at a) 900 MHz and b) 2000 MHz.

ing in most cases deteriorates at the intended operating frequency, thus decreasing the matching efficiency.

The impedance mismatching caused by the user's hand can decrease the total efficiency up to several dBs [3, 62]. In some cases, like presented in [54], the presence of the user can improve the performance of the antenna (total efficiency). In this case the improvement arises from improvement in matching rather than radiation efficiency [55]. Different finger positions with respect to the antenna elements, either active or parasitic ones, have different effects on matching.

When the mechanisms behind the effect of the user are known, a number of technical solutions can be considered to overcome these issues. The locations of the antenna elements in which the loading caused by the user is smaller may be useful particularly with larger device, where space for optimal antenna positioning is more readily available. Another possibility could be to use a broader impedance bandwidth matching, or even adaptive matching [63], so that the antenna would operate in the correct frequency range even with user presence. The use of multiple antenna elements, of which the least effected by the user are selected can be one feasible method for reducing the effect of the user [4]. It is also possible to use so-called antenna shielding, in which one active antenna element is used for communication and another passive element is used as the shield [42]. With this technique, the element with better performance in a particular use case is chosen as the active element.

3. Methods of analysis used and quantities studied

In this chapter, the validation process leading to the choice of suitable simulation software is presented in Section 3.1. Section 3.2 discusses useful quantities and methods of analysis for studying the effect of the device bending. Some estimates of the conceivable changes associated with the shape of the device becoming increasing non-planar are presented in Section 3.3.

3.1 Computational software

It is possible to analyse the performance of antenna structures using different commercial electromagnetic and circuit simulation software. Of the various software available, the FDTD (Finite Difference Time-Domain method) based SEMCAD-X by SPEAG [64], FDTD/FIT (Finite Integration Technique) based CST Microwave Studio [66], FEM (Finite Element Method) based ANSYS HFSS [65], as well as MOM (Method Of Moments) based Mentor Graphics IE3D [67] were chosen as potential candidates for analysing bendable devices. A comparative study using the different software as well as measurements was performed in order to establish the applicability of the individual software to the problem at hand.

Of these four EM simulation software, IE3D is mostly used in this work to design the planar versions of the antenna structures, as it can analyse simple planar metallic (PEC, Perfect Electric Conductor) structures quickly and accurately. Its main drawback is that the software is not very well suited for simulating conformal structures as well as dielectric materials such as the hand of the user. On a general level, when the studied geometry becomes more and more conformal, the different software and the computational algorithms behind them may have limitations (e.g., due to the way in which the software discretises the objects and the surrounding space). It is therefore important to know which (if any?) software can be considered reliable for the study of bendable devices.

The accuracy of the results provided by the different simulation software is verified by constructing two CCE prototypes based on the simulation models, one with 105 mm long ground plane and another one with 175 mm long ground plane. Both cases

use the same type of antenna element, the dimensions of which are shown in Fig. 3.1 along with an example of one of the manufactured prototypes. In the prototypes, the material of the ground plane was 0.15 mm thick copper sheet.

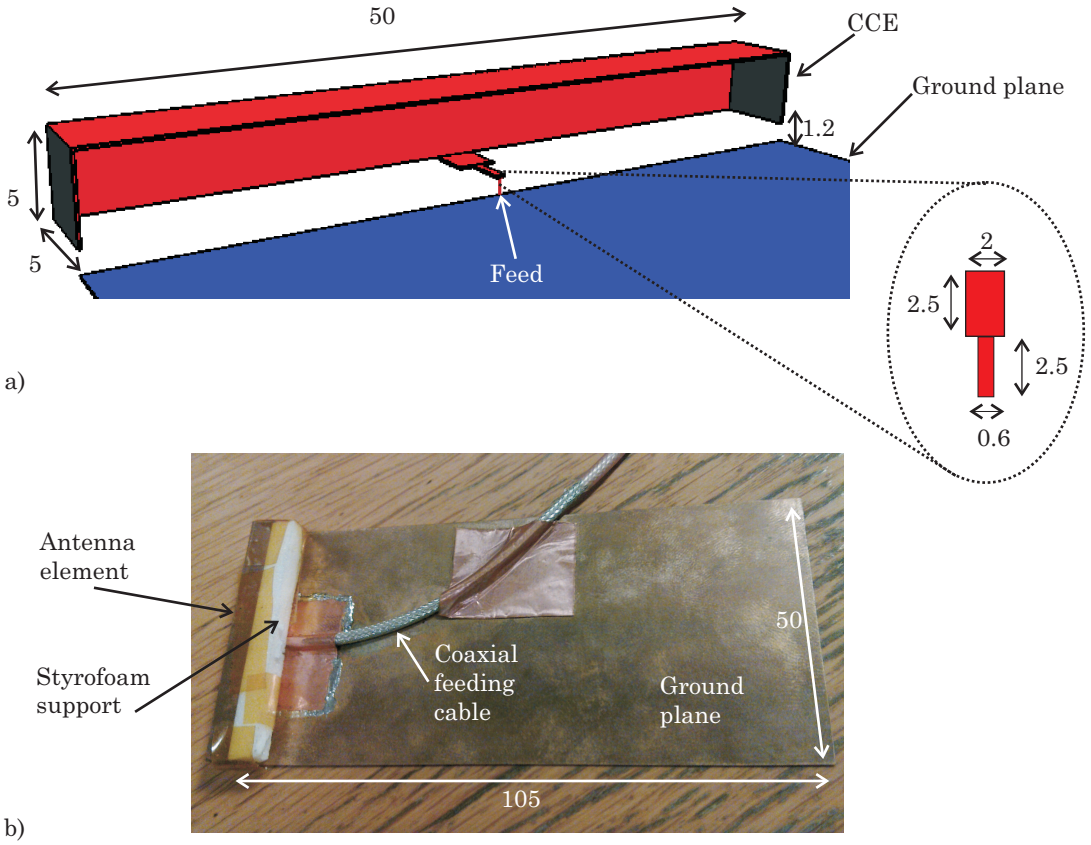

Fig. 3.1. Illustration of the a) antenna element used in the prototypes and b) manufactured prototype for the case of the 50 x 105 mm^2 ground plane. Dimensions in millimetres.

The free space reflection coefficient of the unmatched antennas (i.e. with no matching circuit) is measured with a VNA (Vector Network Analyser) in an impedance box, and the measurement results are compared with those provided by the different simulators in order to see which software (and thereby also simulation method) yields most reliable results. In both simulations and measurements, bending radii of 73.5 mm and 31.5 mm are used. The structures are bent in such a way that the antenna element is positioned outwards with respect to the surface of the cylinder. An illustration of the two bending schemes is given in Fig. 3.2 for the two ground plane lengths. An example of the reflection coefficient results obtained with the different simulation software as well as with measurements are shown in Fig. 3.3. (The reflection coefficients of all different ground plane and bending radius cases considered in the comparison are illustrated in Appendix A.)

When comparing the simulation results, one can see that CST and HFSS generally yield quite similar results whereas SEMCAD has some deviation (particularly with

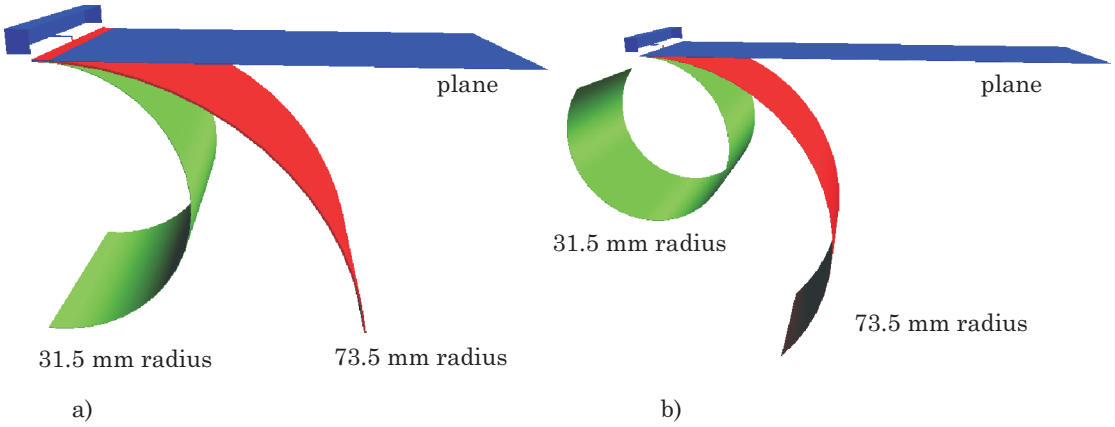

Fig. 3.2. Illustration of the bending schemes for a) 105 mm and b) 175 mm ground plane length.

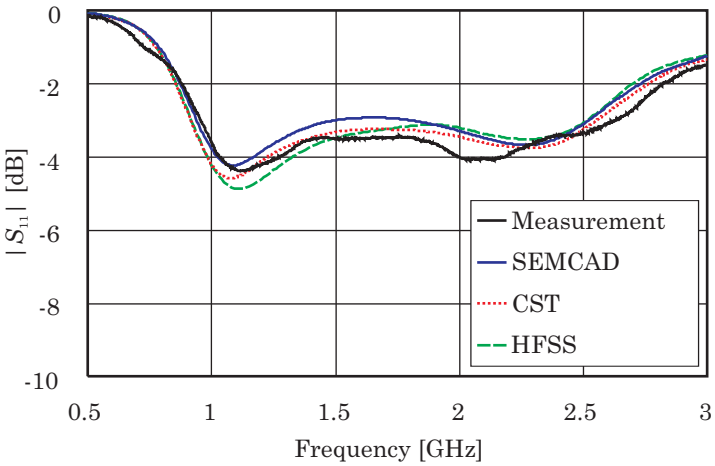

Fig. 3.3. Comparison of simulation and measurement results with the 105 mm ground plane (no bending).

the bent cases). There can be several sources of uncertainty causing the differences between the different simulation and measurement results, such as: 1) simulation error, 2) measurement error, and 3) differences between the simulation model and manufactured prototype.

Firstly, the simulation results may have some discrepancies due to, e.g., the different discretisations used by the computational methods. Like all measurements, the reflection coefficient measurements done with the VNA have always some uncertainty, whose significance can be reduced by performing the measurements carefully. In all the simulation models the antenna structure is bent into cylindrical shape over its entire length.

In the measurements, obtaining a very accurate fitting proved challenging (especially with the shorter ground plane and tighter bending) due to the tensions in the ground plane. With the manufactured prototypes, the fabrication accuracy always influences the obtainable results. Another aspect that affects the measured reflection coefficients is the way that the prototype ground planes are positioned around

the cylindrically-shaped objects used in the measurements. The prototypes are held in place with masking tape, and the more firmly both ends of the antenna structure are in connection with the surface of the cylinder, the better is the agreement with the simulation model – and thereby also the results.

Even though the prototype is manufactured to match the simulation model as closely as possible, the two are nevertheless slightly different – especially in terms of the feeding mechanism. The simulation model has a voltage source between the feeding pin and the ground plane (see Fig. 3.1a) whereas the prototype utilises a coaxial cable to provide the excitation (as shown in Fig. 3.1b). In some cases, the point where the cable is connected to the ground plane (so-called tapping point) can be significant for the response that is obtained from the antenna, because the cable affects the radiation properties of the structure [68].

SEMCAD allows the user to choose between a standard FDTD solver and a conformal FDTD (C-FDTD/FIT) solver, of which the former discretises the structure using a staircase mesh (model consists of small cubic bricks), and the latter produces a conformal mesh. Fig. 3.4 illustrates the difference between the two discretisation schemes available in SEMCAD. Of the two, the staircase voxeling generally requires a considerably larger mesh with bent structures in order to have the same degree of smoothness as the conformal mesh. This is understandable, as accurately approximating round shapes with rectangular blocks is fairly challenging (anyone having tried to build something round using LEGO blocks will agree). In Fig. 3.4, the reason behind the name ”staircase” mesh is clearly visible.

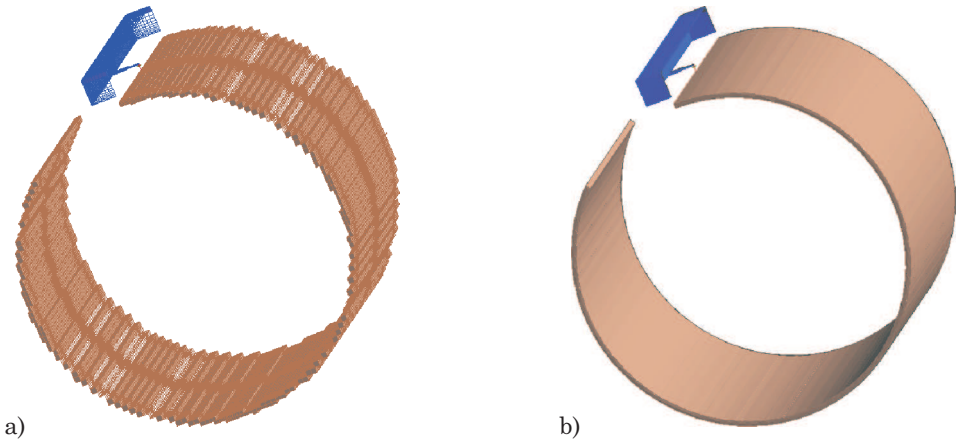

Fig. 3.4. Illustration of the different discretisation schemes used in the simulations with SEMCAD: a) staircase and b) conformal mesh. The example structure is given for the 175 mm ground plane length and 31.5 mm bending radius, as depicted in Fig. 3.2b).

Based on the comparisons discussed above, the software to be used for subsequent simulations was chosen to be SEMCAD. The choice is motivated by three main rea-

sons. Firstly, the agreement between simulation and measurement results can be considered sufficient for the purpose of this work. Secondly, and perhaps more importantly, the RAD department has available both CAD models and physical hand phantoms as well as realistic 3D models of the entire human body for SEMCAD. These models will be highly useful when the antenna structures are bent with the presence of a user. CAD models of the hand can also be applied for CST and possibly also for HFSS, but they are not considered in this work. The third reason for choosing SEMCAD is that we can use top-class hardware acceleration (graphics cards) that increase the simulation speed considerably. Hardware acceleration enables studying very large and accurate simulation setups, including also the user, in a feasible time.

As with the measurements, the non-resonant type antennas are also simulated without external matching components, Their performance is also studied with a matching circuit, due to the fact that non-resonant antennas may display different behaviour in the unmatched and matched impedances when bending the structures. Matching is carried out using Microwave Office circuit simulator developed by AWR [69], and the required component values are obtained using a MATLAB-based tool developed by Mr. Risto Valkonen at Aalto University. This same tool can also be applied for determining the bandwidth potential and the Q_{z} of the different antenna structures studied.

3.2 Methods and quantities to analyse bendable structures

When studying the performance of bendable structures by means of computer simulations and measurements, it is possible to analyse different quantities and parameters in order to better understand the operation. On a general level, it is possible to analyse the structure using antenna or circuit parameters. The requirements of a particular application may determine whether either or both of these approaches should be employed. Often a suitable combination of the two approaches can be useful to obtain the desired information.

The useful antenna parameters include, e.g., the field patterns, directivity and the efficiency of the antenna. Of these, particularly the efficiency is of great importance. In addition to the reasons discussed in Chapter 2, the combination of changes in the shape of the ground plane and the properties of the human tissue might cause wavemodes that do not radiate, meaning that the power lost through them may considerably decrease the radiation efficiency. Also with changing shape, the losses of the ground plane material can become more significant. In this work, all efficiencies

are expressed in decibels (dB) instead of percentages.

Circuit parameters such as impedance, S-parameters or Q provide a different insight into the performance of the antenna. Changes in impedance, either in its real or imaginary part, may be modelled with the equivalent circuit as components having physical meaning, as described in Section 2.3.1. The reflection coefficient (or S_{11} parameter in the case of single-port antennas) can be used to study the changes in the resonant frequency, matching and coupling caused by the bending. Throughout the work, the concept of bending radius is used to describe the amount of bending applied on the antenna structure. This radius corresponds to that of the cylinder around which the ground plane is bent. The planar case (no bending) corresponds to an infinite bending radius. The concept of bending radius is further clarified in Fig. 3.2.

As the radio systems in mobile devices generally employ antennas with fairly low directivity (partly due to the fundamental issue of mobility), one may estimate that the changes in radiation pattern are not the most important consequence of bending the ground plane of the device. In a realistic usage environment, the radio channel has lots of reflections (from e.g. buildings, vehicles and ground) which means that the radio wave reaching the antenna has an ambiguous polarisation. Due to this ambiguity, the polarisation of the antenna has reduced significance. For these reasons, the study of the radiation pattern is omitted in this work. Instead, the main emphasis will be on the circuit properties of the antenna structures. This approach also enables a better use of the equivalent circuit based approach in order to obtain a more profound understanding of the reasons behind the changes that are observed both in free space and with the user.

3.3 Conceivable changes caused by device bending

Before actually proceeding to the study of the planar and bent antenna structures, it is interesting to estimate the different changes that might take place in the antenna performance when the shape of the device becomes increasingly conformal based on a general understanding of antennas and electromagnetics. Different mechanisms or phenomena might occur depending on the frequency as well as on the degree of bending that is applied.

In order to establish the possible frequencies that might be most susceptible to changes in ground plane shape, the coupling element structures of Fig. 3.1 are simulated for the planar, unbent case using IE3D. As was mentioned in the previous

section, some of the current distributions corresponding to different ground plane wavemodes can be more affected by the bending than others. For this reason, the simulations consider both the reflection coefficient and the current distributions. The reflection coefficients obtained for the unbent cases are shown in Fig. 3.5 for both ground plane lengths.

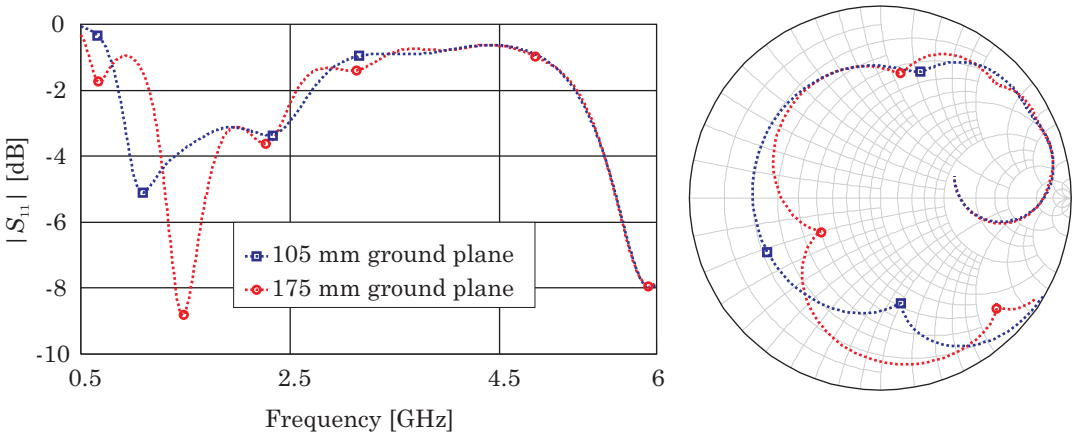

Fig. 3.5. Simulated reflection coefficients in the unbent case for the antenna element shown in Fig. 3.1.

The performance of the antenna element of Fig. 3.1 is also studied in the bent case. In order to perform the comparison, both the planar and bent cases are simulated using SEMCAD, and the obtained unmatched reflection coefficients are shown in Fig. 3.6. As can be seen from the curves of Fig. 3.6, the response of both ground plane lengths is fairly similar beyond 4 GHz for both the planar case and the two bending cases considered.

The curves of Figs. 3.5–3.6 represent the reflection coefficient in the unmatched case, where one can better identify the different resonant frequencies of the ground plane. Based on the reflection coefficient results, the current distributions of the two ground plane lengths are computed with 0.1 GHz interval from 0.5 GHz to 6 GHz in order to see changes in the wavemodes at different frequencies. The behaviour of the current distributions as a function of frequency can be compared with the reflection coefficient data in order to identify the most likely types of the ground plane resonances seen in Fig. 3.5.

When comparing the direction of the currents at different frequencies to the schematic illustrations given in Fig. 2.6, one can see that for the 105 mm long ground plane, the first resonance at around 1.2 GHz is of Type 1 (current flowing in one direction along the broad side of the ground plane). Around the second resonant frequency (2.4 GHz), the current distribution begins to take the shape of Type 3, meaning that there is a null in the middle of the ground plane. At frequencies above 5 GHz, the current

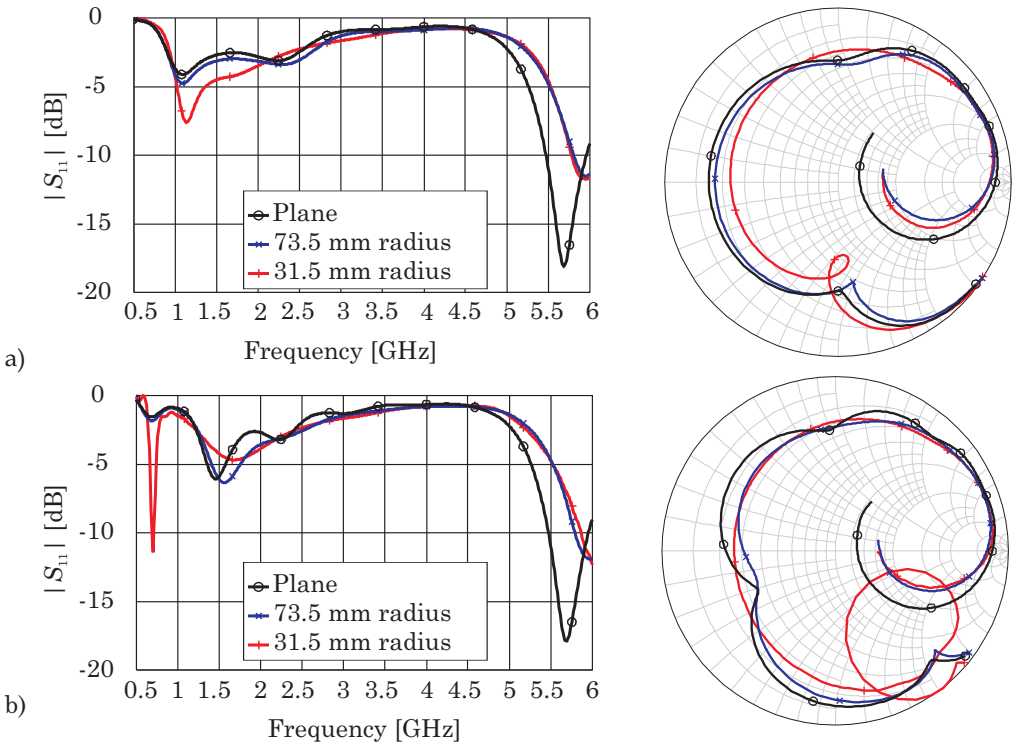

Fig. 3.6. Simulated reflection coefficients for a) 105 mm and b) 175 mm ground plane length.

distribution does not directly correspond to any of the types shown in, e.g., [52, 53], which indicates that the distribution is some kind of a hybrid between the antenna element and ground plane current modes. An illustration of some of the current distributions that can be seen with the 105 mm ground plane are shown in Fig. 3.7.

The lowest-order resonance of the longer ground plane, at 0.7 GHz has a current distribution of Type 1, and Type 3 is excited at around 1.5 GHz. With increasing frequency, the number of nulls along the ground plane increases, with two at around 2.3 GHz, three around 3.1 GHz and four around 4 GHz (so-called higher-order modes). At 5 GHz and higher frequencies, the current distribution of the longer ground plane is similar to that of the shorter ground plane, and the reflection coefficient is nearly identical to that of the shorter ground plane. The latter observation is actually true already from 4 GHz onwards. Examples of the current distributions that are observed with the 175 mm ground plane are depicted in Fig. 3.8.

By looking at the current distributions at the different frequencies, it is clear that the type of coupling element used does not excite currents along the short edge of the ground plane (Type 4 in Fig 2.6). This is due to the fact that the coupling element used is centre-fed. If the feed were to be placed to the corner of the ground plane, also currents directed along the short-edge could be created.

Generally, the exact type of the current distribution depends on the type and positioning of the feeding element, the symmetry of the position of the element with

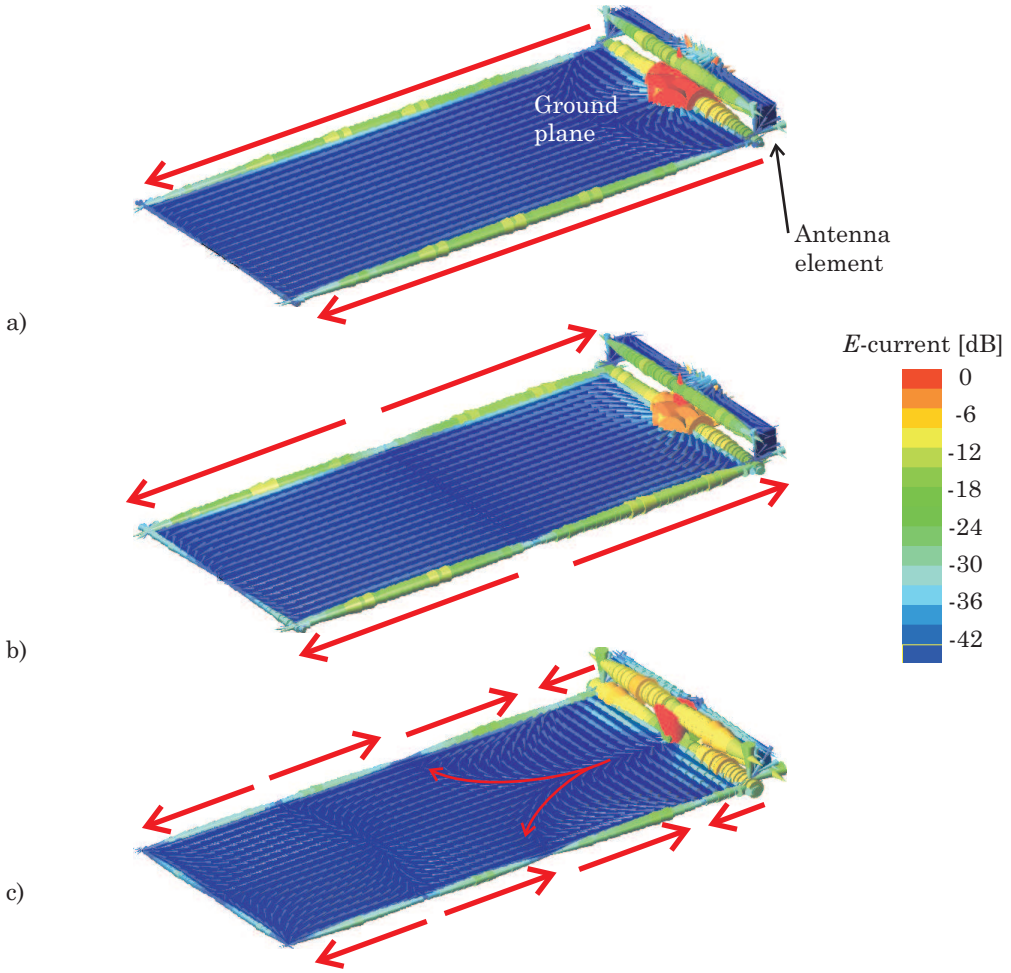

Fig. 3.7. Simulated current distributions for the 105 mm ground plane at a) 1.2 GHz, b) 2.4 GHz, and c) 5.1 GHz.

respect to the ground plane, positioning of the feeding pin on the element and so on. The current modes reported in [52] have been calculated using the horizontal and vertical dipoles (more symmetric structure). Additionally, the geometry of the ground plane (overall dimensions, ratio of broad and narrow sides etc.) also has an effect, both on the resonant frequencies and the type of the current distributions that can be created.

Based on the current distributions and unmatched reflection coefficients one may consider the frequencies at which the mobile device could be most sensitive to changes in the shape of the ground plane. These frequencies are most likely near the resonant frequencies of the ground plane wavemodes. The different directions of the currents may indicate different responses to changes in the shape of the ground plane. This aspect will become more clear once the structure is actually bent. Now that the possible locations of the changes have been identified, one may contemplate what the changes might be and what could be causing them.

When the ends of the ground plane are brought closer to each other by bending the

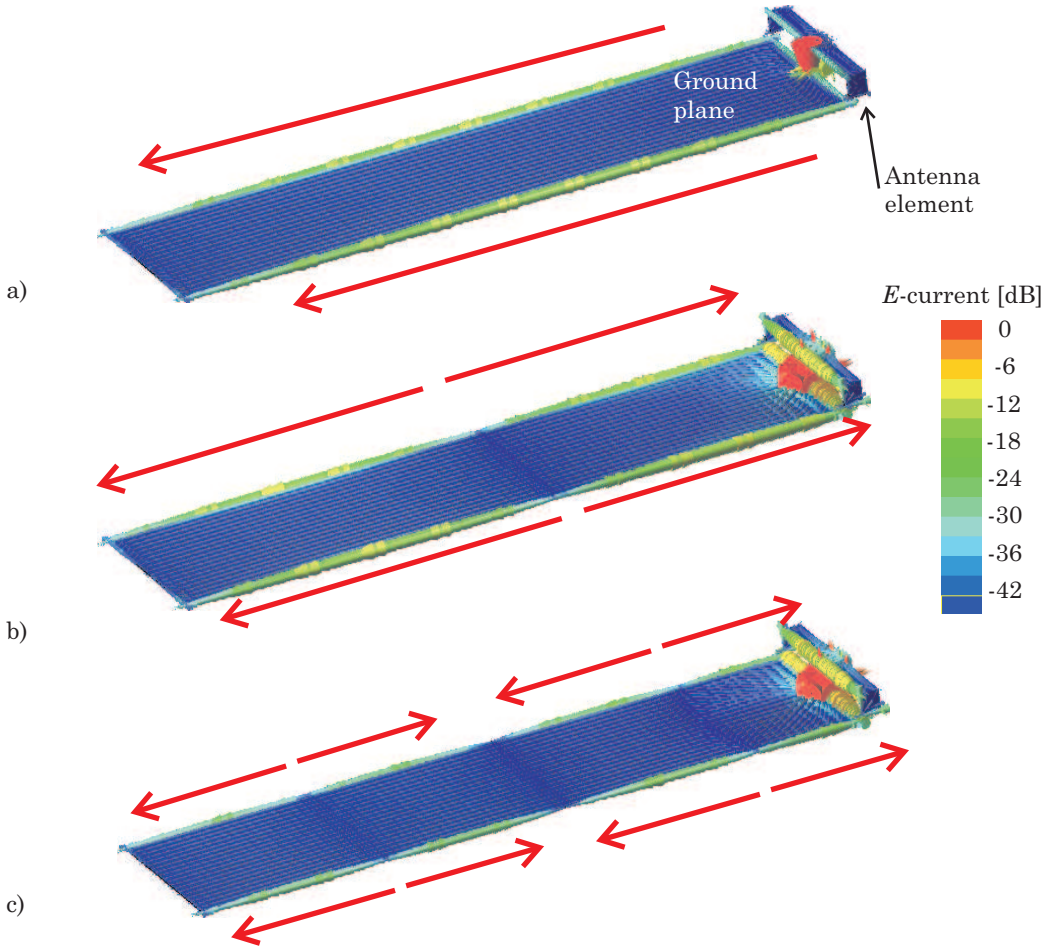

Fig. 3.8. Simulated current distributions for the 175 mm ground plane at a) 0.7 GHz, b) 1.5 GHz, and c) 3.1 GHz.

structure, it is possible that the performance of the antenna is disturbed by additional coupling between the ends. This effect will be analysed later with the equivalent circuit. The closer the ends are, the larger the effect most likely will be. The source of this coupling may be increasing capacitance between the two ends. A somewhat analogous case is the equivalent circuit for a slot in basic microstrip lines, in which the slot is modelled with a π-type network consisting of both series and shunt capacitances. Additionally, when the ground plane is bent into a more curved shape, this can also change the current paths of the surface current distributions, which can cause additional inductance.

In a conventional planar mobile device, the current distribution depends on the wavemode that is excited. The possible changes in the current distribution when the shape of the structure changes can mainly be considered to be detrimental. They might include, e.g., the cancelling out of opposite-directed currents with an increasing degree of bending. This in turn weakens the radiation properties of the device.

The importance of the changes of the current distribution most likely depends on

frequency, as well as on the type of the antenna element used (resonant or non-resonant type). If the main radiator in the antenna structure is the antenna element, as is the case with, e.g., PIFAs, the effect may be less significant than with non-resonant coupling elements that are mainly used to couple to the ground plane wavemodes. Another important difference between resonant and non-resonant type antennas is that the former has an inherent matching circuit, which can make distinguishing the changes caused by the ground plane shape more difficult (which part of the changes is caused by the shape of the ground plane itself, and which are a result of changes in the ”matching circuit”). With non-resonant unmatched antennas, the majority of the changes are directly caused by changes in the ground plane wavemodes. The frequency also affects to the radiation contribution of the ground plane, as was explained in the previous chapter.

When bending the ground plane of the mobile terminal, the effect of the lossy dielectric material of the hand will most likely consist of such changes that are already present when a rigid mobile device is held in the hand, as well as changes that are specific for the bent cases. The effects include the shift of the resonant frequency and the decrease in efficiency. It is possible that the changes caused by the hand may be more profound than with planar devices.

Compared to the planar case, the efficiency may change more severely, due to reduced radiation caused by changes in the current distribution as well as due to the power that is absorbed into various parts of the hand (the tissue absorption depends also on the usage mode, such as browsing or wrist mode). These usage modes are explained in greater detail in Chapter 4. Some of the effects that occur first when placing the hand near the antenna structure can be identified when comparing a particular case when the user is present to the corresponding free space case.

Apart from the effects described above, there could be also other changes that are first observed when the device is bent and the different quantities have been analysed. These kinds of changes will then be considered in subsequent chapters.

4. Antenna performance in planar and bent antenna structures

In this chapter, the performance of coupling element type antenna structures is studied in typical use cases, meaning that the presence of the user is also taken into account. With traditional rigid mobile devices, the effect of the user can be studied using different hand grips such as talking grip or browsing grip. Also the effect of the head (with or without the talking grip) can be considered, especially in *SAR* studies. In the case of bendable devices, the talk mode is of lesser concern, and it is therefore not considered here. The results obtained in this section can also be used to verify some of the predictions on the performance given in Section 3.3.

It is possible to bend the mobile device in or around the hand in a large number of ways. Two distinct types of bending are considered here: browsing mode and so-called wrist mode. The browsing mode is used for describing similar use as with conventional devices, but flexibility enables also some additional possibilities. By applying different bend gestures, the user can perform different functionalities with the device, as discussed in [71]. In the wrist mode, the ground plane of the device is simply bent around the wrist of the user.

This chapter is organised as follows. Section 4.1 presents the different antenna elements and element locations, bending cases and hand models used in the study. The performance of the antenna elements in the free space case with and without the matching circuit is studied in Section 4.2. The effect of the user is studied in both browsing mode and wrist mode, and the results are presented in Sections 4.3 and 4.4, respectively. Finally, the modelling of the bending in free space with the resonator-based equivalent circuit is studied in Section 4.5.

4.1 Antennas, bending cases and hand models studied

4.1.1 Antenna elements

When analysing the effect of ground plane bending both in free space and with the user present, the antenna elements that are used in the study are CCEs, whose di-

mensions are designed in the unbent case. Both on-ground and off-ground positioned antenna elements are considered (see Fig. 4.1), in order to study if a certain element location type is more sensitive to the effects of bending. The principal difference of on-ground and off-ground elements is (as one might guess based on the name) that the on-ground element is situated completely above the ground plane. In recent years, off-ground elements have gained increasing interest in mobile terminal antenna design and research. One reason is that the off-ground element can be made smaller (both in terms of element area and height) than an on-ground element, and the bandwidth can be the same.

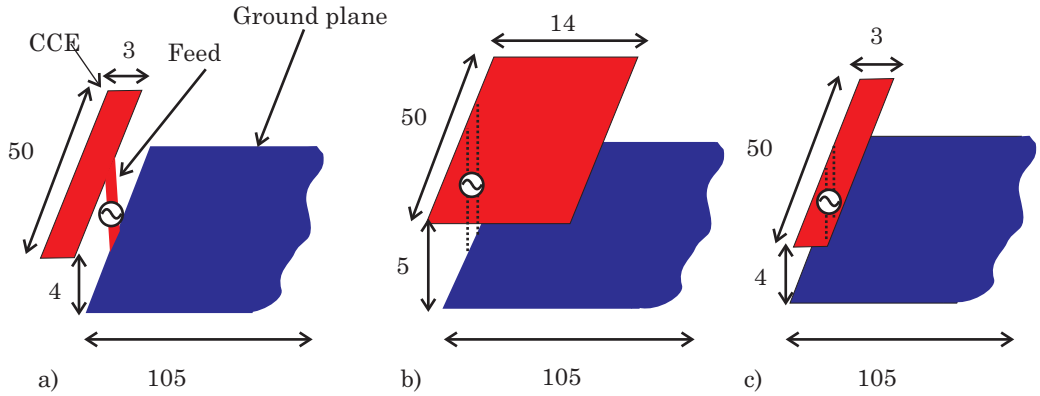

Fig. 4.1. Different antenna cases studied: a) CCE#1 (off-ground), b) CCE#2 (on-ground) and c) CCE#1 (on-ground).

Initially, an off-ground positioned coupling element, CCE#1 (off-ground) is designed using IE3D and SEMCAD. The dimensions of the element are 3 x 50 x 4 mm^3 [length x width x height] (see Fig. 4.1a). The starting point of the design is the frequency specifications of the GSM900 system (see Table 1.1). The bandwidth of the antenna element at that frequency range should be large enough to cover the uplink and downlink bands of the system simultaneously, and still be sufficiently narrow so that the response of the antenna element to the bending can be seen more clearly. With too large a bandwidth, the bending may not be a problem because the antenna may still remain in-band regardless of the bending.

When the CCE#1 (off-ground) element was placed on-ground, the bandwidth performance at the 900 MHz band clearly decreased. The reason for this change is related to the fact that the electric field strength is larger beyond the edge of the ground plane. A larger field strength enables larger coupling, which means that an off-ground positioned antenna element has better performance bandwidth-wise than an on-ground element of equal dimensions [48]. Therefore, the element was made larger, both in terms of element area and height. The resulting element is referred to as CCE#2 (on-ground), shown in Fig. 4.1b, and its dimensions were tuned in such a

way that CCE#1 (off-ground) and CCE#2 (on-ground) antenna structures would have roughly the same Q_{z}. This last condition is applied in order to make the comparison between the elements more fair: because the two elements are different, it can be difficult to determine what part of the changes observed is related to the position of the element, and what is caused by the difference in size. With similar Q_{z}, the elements have similar bandwidth performance, as indicated by Eq. (2.4).

In order to further improve the comparison, the antenna element CCE#1 is also positioned on-ground (see Fig. 4.1c), even though this results in a loss of bandwidth. However, a direct comparison to the off-ground version is made easier because the elements are the same. In this case, the most significant reason behind the different response of the element is the location of the element itself.

One important point to notice is that the dimensions of the antenna elements are optimised based on the specifications of a single radio system. Therefore, the bandwidth performance at other frequency bands may or may not meet the needs of the corresponding systems. A multiband optimisation of the bandwidth is possible, though this process is fairly complicated and might not result in an improved overall understanding of the fundamental reasons behind the effects of the bending.

4.1.2 Bending cases

In principle, a ground plane can be bent in a large number of different ways, depending partly on its dimensions, the rigidity of the material and so on. It is also possible to bend the ground plane along all three coordinate axes, e.g., onto a spherical surface. In this work, all of the bending cases feature bending only along one axis. The choice is made partly based on the different use cases and related applications that are considered, but also in order to simplify the required modelling in the EM simulator. The two use cases studied, browsing mode and wrist mode, give rise to slightly different bending regimes from the practical point-of-view. In the browsing mode, both the 105 mm and 175 mm ground planes can be bent in the same way by using the different bending radii. For the wrist mode, the number of practical bending radii is limited by the fact that a real device (including the casing) has to be secured firmly around the wrist.

The different bending radii considered for the shorter and longer ground plane are illustrated in Figs. 4.2 and 4.3, respectively. The smallest radius is determined by the length of the ground plane, as any radius that results in a smaller circumference than the ground plane length will result in overlapping of the ends of the ground plane, which is not practical. In the case of the 105 mm ground plane, the lower limit

for the bending radius is 16.7 mm, and in the case of the 175 mm ground plane, the corresponding value is 27.9 mm. For this reason, the lower limits for the bending radius were chosen to be 20 mm and 30 mm, respectively, for the shorter and longer ground planes (see Figs. 4.2 and 4.3).

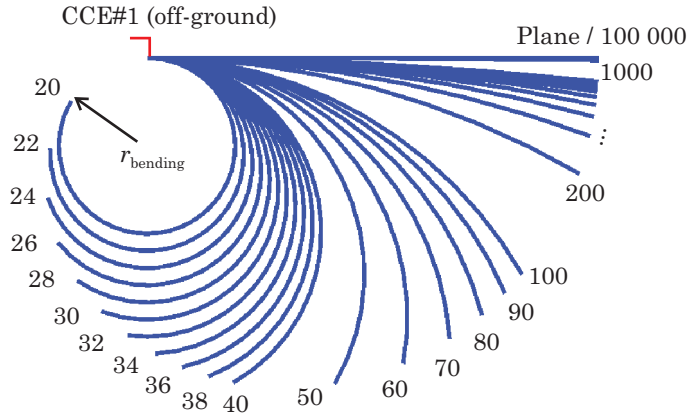

Fig. 4.2. Bending radii studied with the shorter (105 mm) ground plane (shown for the CCE#1 (off-ground) antenna element).

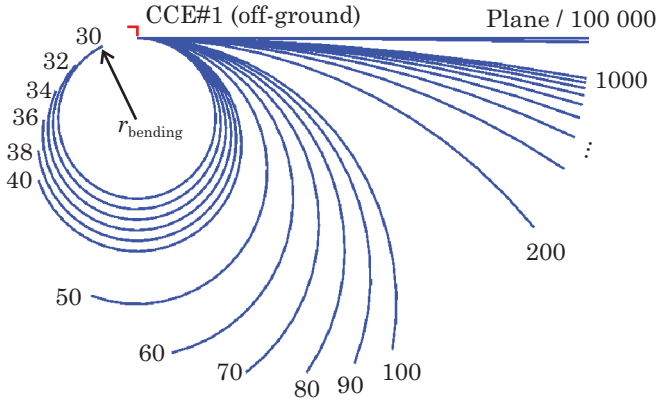

Fig. 4.3. Bending radii studied with the longer (175 mm) ground plane (shown for the CCE#1 (off-ground) antenna element).

As can be seen in the figures, the smaller radii are studied with smaller steps. The reason for this is the fact that the more significant changes are likely to occur with a smaller bending radius. The larger values are included because the behaviour of the bent structure should asymptotically approach that of the planar case with increasing bending radius (a plane can be modelled as a cylinder having an infinite radius). For the sake of practicality, the largest bending radius is limited to 100 000 mm, which already provides a very accurate approximation of the planar case.

4.1.3 Modelling of the hands in electromagnetic simulations

The human hand can be modelled in electromagnetic simulations with an increasing degree of realism, ranging from simple dielectric block type models to complex, posable hand models that include, e.g., skin, fat, muscle and bones. Different tissue types have different properties, including density and electrical parameters, that can affect the antenna structures in different ways.

Among the most important electrical parameters contributing to the effect of the tissue on antenna performance are relative permittivity (ϵ_r, dimensionless) and electrical conductivity (σ, [S/m]). Both permittivity and conductivity are dispersive parameters, meaning that their values are frequency-dependent. Other factors, such as the moisture of the hand, also contribute to the values of permittivity and conductivity (especially conductivity). Values for permittivity and conductivity have been tabulated, e.g., in [72], based on the properties of a dry hand. Other sources, such as [73] report values that are an average of those for dry and moist tissue.

In this work, so-called dispersive hand parameters are used. They are based on the values reported by CTIA [72] and are valid in the frequency range from 300 MHz to 6 GHz. The dispersive model uses three dispersive electric poles to compute or fit the correct permittivity and conductivity values also for frequencies between the tabulated values of [72]. An alternative to the dispersive parameters would be to apply the values at a point frequency over a broadband sweep. However, this approach will result in some inaccuracies because it will (partly depending on the frequency) over- or underestimate the effect of the hand, something that can be minimised using dispersive values. However, the dispersive hand parameters do not support the conformal FDTD solver in SEMCAD which means that the standard FDTD solver has to be applied even for the bent structures (causing an increase in simulation time due to the finer mesh required).

4.1.4 Hand models in the browsing and wrist modes

The dimensions of the hand models used in this work represent those of an average human hand (shown, e.g., in Figs. 4.4–4.5), and they are based on comprehensive anthropometric studies (e.g. [74]). The CAD models of the hands are provided by SPEAG, and as explained in Chapter 3, their availability is one significant reason for performing the user effect studies with SEMCAD. The hand models used with the browsing grip (both left and right hand) are illustrated in Fig. 4.4. Both hands are used because it is assumed that the materials used in the devices have no memory

effect, meaning that they return to their natural shape once the grip is released. With a suitable ground plane material, also a single-hand browsing grip could be considered (not studied here).

Fig. 4.4. Left and right hand models used in the two-hand browsing mode. The size of the hand corresponds to that of an average human hand.

The hand model used for the wrist mode is shown in Fig. 4.5. In this model, the wrist is modelled using a cylinder whose radius is 28 mm. This assumption differs slightly from a real human wrist in two ways: the shape of the real wrist is rather elliptical than cylindrical, and also the thickness gradually increases when going towards the elbow. However, the choice that is made can be justified for two main reasons. Firstly, it is easier to bend the ground plane about a symmetrical shape in the simulator. Secondly, the symmetry of the cylinder means that a fairly even loading from the hand on the ground plane can be achieved. Considering an actual device and wrist, the distance between the two is most likely not constant, but the average overall effect could be the same as with a symmetric case. An additional benefit of the chosen wrist size is that the circumference of the 28 mm cylinder is roughly 176 mm, which is fairly close to the mean circumference of a real male hand. As given in [74], the values are 174.3 mm and 151.4 mm for male and female hand, respectively.

Fig. 4.5. Hand and wrist model used in the wrist mode. The size of the hand corresponds to that of an average human hand, but the length of the cylindrical wrist is only indicative.

The gap between the wrist and the ground plane can be adjusted with a suitable bending radius. Considering a practical bendable device, the ground plane is very likely not in direct contact with the wrist of the user (due to, e.g., the casing of the device). For this purpose, the ground planes are bent around the wrist in such a way that the air gap between the ground plane and wrist is 2 mm, which can be consid-

ered feasible for practical applications. This is achieved with a bending radius of 30 mm (wrist radius 28 mm). The device is positioned symmetrically about the wrist, meaning that the distance between device and wrist is constant in all directions.

In the browsing mode, the different applications or user preferences can affect to the required bending radius. The wrist mode is ”fundamentally” different because the device has to be placed around the wrist of the user (making too large or too small bending radii infeasible). For this reason, the dimension to be modified in the wrist mode is the length of the ground plane. The minimum and maximum lengths to be considered are 105 mm and 175 mm, respectively.

The maximum length is obviously determined by the dimensions of the wrist, as the length has to be smaller than the wrist circumference. The minimum length must be bendable around the wrist, and it should be able to support the bandwidth requirements of the different systems. The 105 mm length is chosen for the sake of convenience. An issue worth considering is the limit at which a device can truly be called bendable (or when the bending still remains a problem). When the dimensions approach those of, e.g., a wrist watch, the main problem gradually reduces to that of reactive loading caused by the tissue. This problem is familiar from the design of conventional mobile terminals.

The studies in the wrist mode are performed for ground plane lengths from 105 mm to 175 mm, using 10 mm steps. These cases are illustrated in Fig. 4.6, in which also the cylinder modelling the wrist is visible. The purpose is to locate an optimal length for the ground plane when it is positioned in the vicinity of the user. For all ground plane lengths, both the planar and bent versions are studied in free space. The different lengths are compared in such a way that the planar version of a given ground plane is matched to the desired frequency in free space, and the same matching circuit is then applied to the bent structure (both in free space and in the presence of the hand).

4.2 Capacitive coupling element structure bent in free space

In this section, the performance of the antenna elements of Fig. 4.1 in the different bending cases of Figs. 4.2 and 4.3 is compared. The main emphasis is on the performance of the antenna structures in the unmatched case (Section 4.2.1), but also some observations are made regarding the comparison of the different cases when a lumped element matching circuit is used to obtain a resonance at a desired frequency (Section 4.2.2).

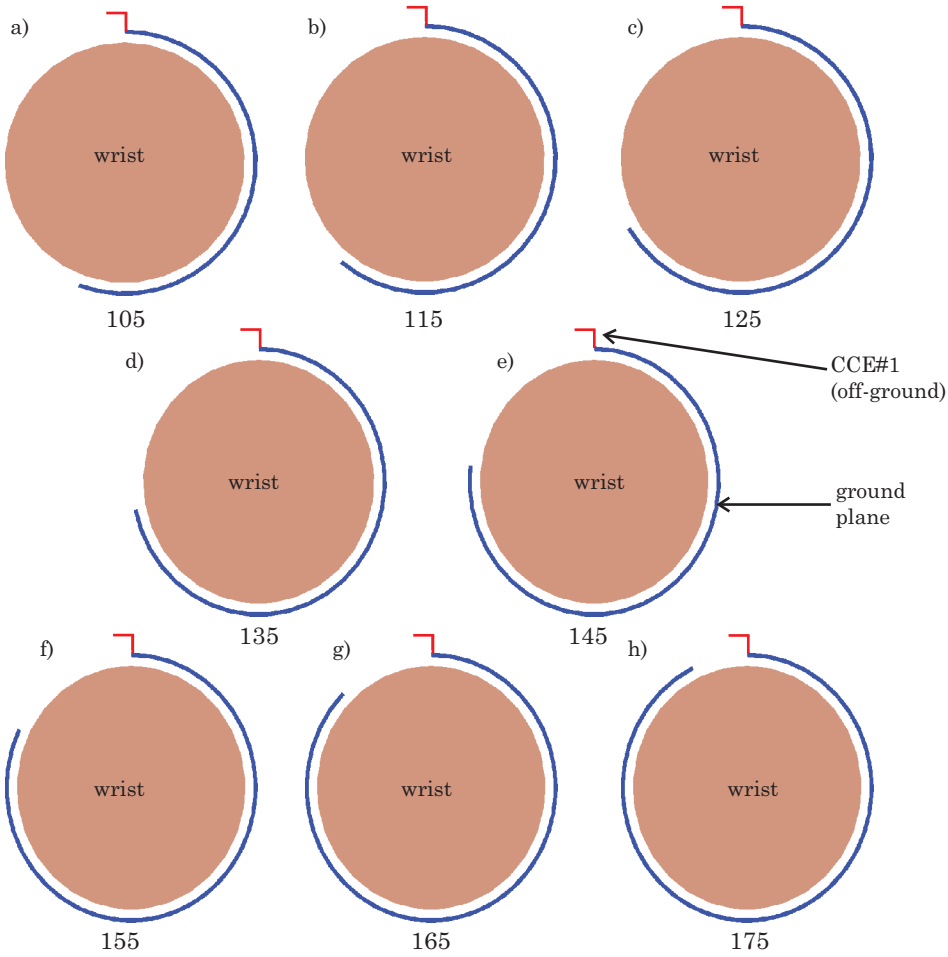

Fig. 4.6. Illustration of the different ground plane lengths considered in the wrist mode: a) 105 mm, b) 115 mm, c) 125 mm, d) 135 mm, e) 145 mm, f) 155 mm, g) 165 mm, and h) 175 mm. In all cases, the air gap between ground plane and wrist is 2 mm. The radius of the wrist is 28 mm.

4.2.1 Effect of the bending in the unmatched case

In order to observe the changes that can occur when an unmatched mobile terminal antenna structure is bent, it is possible to consider different approaches by means of different quantities. By looking at the unmatched reflection coefficient (S_{11}) curves, the general behaviour of the different resonant wavemodes of the ground plane can be observed. Certain wavemodes can be such that the resonance is not affected by the changes in the shape of the ground plane. In other words, the data can reveal the most sensitive frequencies that should be studied also in the matched case.

For practical applications, the CCEs are always matched to the desired frequency band, and the associated impedance bandwidth requirement is based on the specifications of the radio system. For this reason, the bandwidth performance is of significant interest for the different bending radii. A measure for the bandwidth that can be obtained with the antenna in a particular bending case can be calculated from the Q. This is due to the inversely proportional relation between BW and Q, as discussed in

Section 2.2.2. By using Eq. (2.4), the actual bandwidth can also be calculated from the Q.

The Q_z calculated from the simulated input impedance of the antenna structure with the 105 mm ground plane is shown in Fig. 4.7a for the 920 MHz case, and in Fig. 4.7b for the 1920 MHz frequency. Similar curves for the 175 mm ground plane case are given in Fig. 4.8.

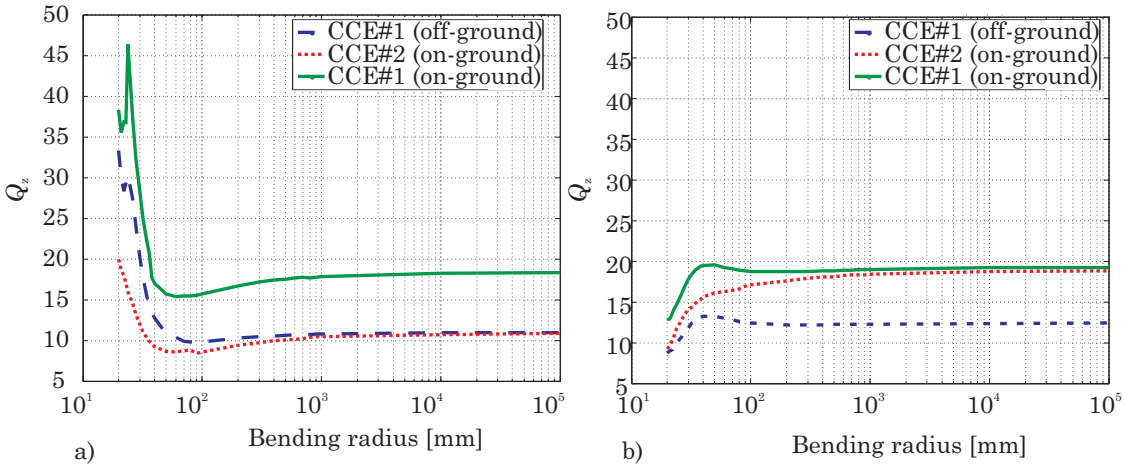

Fig. 4.7. Calculated Q_z for the 105 mm ground plane at a) 920 MHz and b) 1920 MHz frequency.

From the curves of Fig. 4.7 it is possible to see that the CCE#1 (off-ground) and CCE#2 (on-ground) elements have the same Q_z in the planar case (as they were designed to), and that beyond the 1000 mm bending radius the difference between the bent and planar cases is fairly small. Both the on- and off-ground positioned CCE#1 elements display an interesting dip in their Q_z curve between 20 mm and 30 mm bending radius. This phenomenon was first observed when using the bending radii of Fig. 4.2. However, some additional bending radii between 20 and 25 mm were used, and these cases verified that the dip truly does take place and is not, e.g., simulation error. A slight dip can also be seen in the Q_z curve of the CCE#2 (on-ground) element. At 1920 MHz, the range of variation of the Q_z values is smaller with both ground plane lengths than at 920 MHz.

With the longer ground plane, the behaviour of the Q_z at 920 MHz shows an opposite trend than with the 105 mm ground plane, meaning that the Q_z is reduced as more tighter bending is applied. All antenna elements have an increase in the Q_z at 920 MHz as the bending radius approaches 30 mm, and this increase is most noticeable in the CCE#1 (on-ground) case (as this antenna element is too small to provide sufficient coupling in the on-ground case).

The considerably larger Q_z at the lower frequency with the longer ground plane is due to the fact that this ground plane experiences a local minimum of the bandwidth

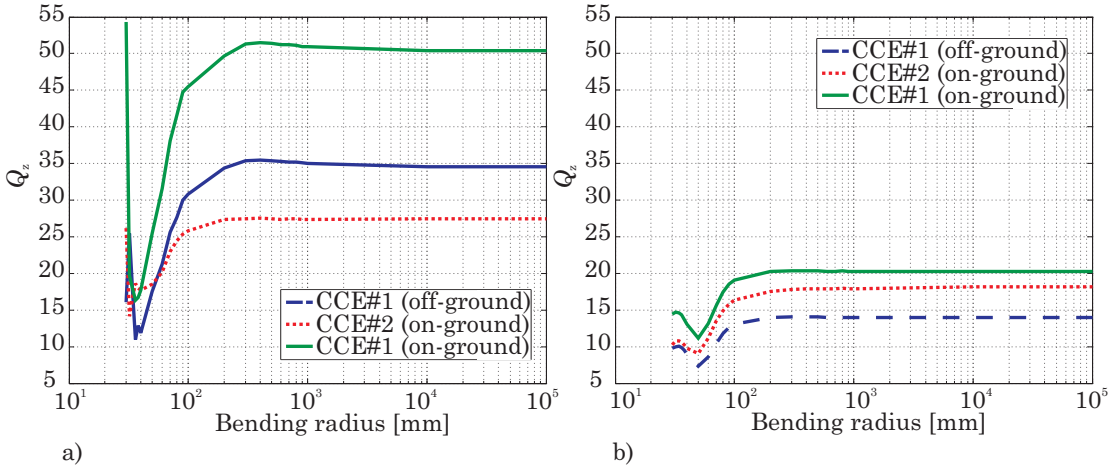

Fig. 4.8. Calculated Q_z for the 175 mm ground plane at a) 920 MHz and b) 1920 MHz frequency.

potential around 1 GHz. For this reason, subsequent studies with the 175 mm ground plane will also consider the 722 MHz frequency (centre frequency of the lower LTE 700 band, see Table 1.1). This frequency provides better bandwidth performance as it is closer to the first resonant frequency of the 175 mm ground plane (located around 0.7 GHz, see, e.g., Fig. 3.5).

At 920 MHz, all three antenna elements have a region between 30 mm and 100 mm bending radius in which the Q_z is lower compared to the planar case for both ground plane lengths (with the longer ground plane, this region is even broader, going up to 200 mm). As was explained in Section 2.2.2, the Q and bandwidth are inversely proportional. This would suggest that by applying a bending radius within the 30 to 100 mm range could provide the antenna structure with a broader impedance bandwidth than in the planar case.

The possible reasons for this observed behaviour could be related to a decrease in the reactive (capacitive and/or inductive) energy stored in the near field of the antenna structure, or to an increase in the losses. As the simulated structure is modelled as PEC (no conductive losses), the only source for these losses is through the radiation resistance of the different wavemodes (see Section 2.3.2). An analysis of the bending with the equivalent circuit model (see Section 4.5) can provide further clarification into this matter.

4.2.2 Effect of the bending with matched antenna elements

An alternative to studying the bandwidth of the antennas based on the Q is to see how the bandwidth with respect to a particular matching criterion (e.g. –6 dB) changes according to the shape of the ground plane. For this purpose, the different coupling elements of Fig. 4.1 are critically matched to the frequencies of interest using a

two-element matching circuit. The component values of the matching circuit are determined for the unbent case, and the same component values are applied also for the different bending cases.

However, this approach has its limitations because of the actual matching circuit. As there are two or four possible circuit topologies (see Fig. 2.3), they all possibly result in slightly different bandwidth in the unbent case. Furthermore, when the ground plane is bent, the critical matching of the unbent case will inevitably deteriorate. Therefore, it may be difficult to distinguish the between the changes that are caused by the actual change in the shape and those that are associated with the matching not being any more critical.

The choice of the critical matching is justified because it provides more narrowband performance, which makes the changes due to the bending more visible. In practice, though, optimal matching is more commonly used than critical matching, because of the more broadband behaviour (see Fig. 2.4).

4.3 Capacitive coupling element structure bent in browsing mode

In this section, the performance of the CCE structures in the two-hand browsing mode is studied. There is a large number of different bending cases, as shown, e.g., in Figs. 4.2–4.3, but not all of these are practical for hand-held applications (especially at the lower end of the range). In the following, a bending radius of 73.5 mm is considered for both the 105 and 175 mm ground plane lengths (see Fig. 3.2). The two antenna elements that are considered are the CCE#1 (off-ground) and CCE#2 (on-ground) elements (shown in Fig. 4.1), and they are studied in the unmatched case.

The calculated Q_{z} for the antenna elements are given in Tables 4.1–4.2 for the CCE#1 (off-ground) and CCE#2 (on-ground) elements, respectively. Of the lower band frequencies, 920 MHz is used with the 105 mm ground plane and 722 MHz with the 175 mm ground plane because the 920 MHz frequency with the longer ground plane has too small bandwidth potential.

The values of Tables 4.1–4.2 show that with both antenna elements, when the hand is introduced into the model, the Q_{z} increases at the lower frequencies (920 MHz and 722 MHz). At the 1920 MHz frequency, the hand causes considerable reduction in the Q_{z}. The behaviour at the lower band appears a bit counter-intuitive due to the additional losses introduced by the conductivity of the hand. They should, according to Eq. (2.5), reduce the Q as the denominator increases. However, there can be also

Table 4.1. Calculated Q_z in the two-hand browsing mode for the CCE#1 (off-ground) antenna element. In the "plane" case, a two-hand grip is applied to the ground plane without any bending, and in the "browsing" case, the grip is otherwise similar except for the 73.5 mm bending radius that has been applied. The term "fs" refers to the free space case (no hands).

f	105 mm (plane)		105 mm (browsing)		175 mm (plane)		175 mm (browsing)	
[MHz]	Q_z	Q_z (fs)	Q_z	Q_z(fs)	Q_z	Q_z (fs)	Q_z	Q_z (fs)
722	–	–	–	–	19.3	10.1	10.7	7.3
920	13.9	11.1	11.8	10.1	–	–	–	–
1920	6.7	12.6	6.6	13.0	6.4	14.2	3.7	11.1

Table 4.2. Calculated Q_z in the two-hand browsing mode for the CCE#2 (on-ground) antenna element. In the "plane" case, a two-hand grip is applied to the ground plane without any bending, and in the "browsing" case, the grip is otherwise similar except for the 73.5 mm bending radius that has been applied. The term "fs" refers to the free space case (no hands).

f	105 mm (plane)		105 mm (browsing)		175 mm (plane)		175 mm (browsing)	
[MHz]	Q_z	Q_z (fs)	Q_z	Q_z (fs)	Q_z	Q_z (fs)	Q_z	Q_z (fs)
722	–	–	–	–	3.6	9.3	4.5	5.2
920	4.1	10.6	3.6	8.7	–	–	–	–
1920	5.7	16.2	5.6	16.5	5.3	16.0	5.2	14.2

other mechanisms affecting the Q, and which may be identified through the wrist mode studies (Section 4.4) or when modelling the bending using an equivalent circuit (Section 4.5).

In addition to the Q_z, which also gives insight into the bandwidth performance of the antenna structure, the presence and properties of the hand also have an effect on the efficiency. Table 4.3 shows the effect that the bending of the ground plane has on the η_{rad} in the different cases studied. In the free space case, η_{rad} is ideally 0 dB because the antenna structures are simulated as PEC (no losses). Therefore the reductions seen in the tabulated values in Table 4.3 are caused by the absorption of the radiated power into the hands.

The values of Table 4.3 show that the absorption to the hands can vary more than 1 dB, and that in some cases, the bent ground plane improves the η_{rad}. When bending the ground plane, the current distributions of the ground plane wavemodes change, and depending on the exact type of the bent current distribution, the radiation performance can either improve or degrade. In addition to or as a consequence of the changing current distribution, it may also be so that the directional pattern of the

Table 4.3. Simulated η_{rad} (in dBs) for the different cases with the two-hand browsing grip. In the "plane" case, a two-hand grip is applied to the ground plane without any bending, and in the "browsing" case, the grip is otherwise similar except for the 73.5 mm bending radius that has been applied.

	CCE#1 (off-ground)			CCE#2 (on-ground)		
Case	722 MHz	920 MHz	1920 MHz	722 MHz	920 MHz	1920 MHz
105 mm (plane)	−2.1	−2.8	−3.0	−2.6	−3.3	−3.1
105 mm (browsing)	−1.7	−3.0	−2.4	−2.3	−3.6	−2.5
175 mm (plane)	−1.7	−3.0	−2.5	−2.4	−3.5	−2.6
175 mm (browsing)	−2.6	−3.8	−1.3	−3.1	−4.1	−1.8

antenna changes. This can lead to the antenna radiating more into directions that are not covered by the hands, hence resulting in less absorption into the tissues. The largest improvement in the performance occurs with the CCE#1 (off-ground) element and 175 mm ground plane at 1920 MHz, in which case the improvement is 1.2 dB compared to the planar case. The most detrimental effect of the bending in the hand can be seen at 722 MHz in the case of CCE#2 (on-ground) with 175 mm ground plane. This situation results in additional absorption of 0.7 dB.

One could expect that the effect of the hand absorption gets more severe with a tighter bending radius, and less severe when a looser bending is applied. However, as was mentioned earlier, the tightest bending cases with likely the most significant problems caused by the bending are also the least practical ones. If, on the other hand, the bending radius is further increased, the study eventually approaches that of the performance of planar mobile terminals in the browsing mode (results for this topic can be found in the literature, e.g., in [5, 75]).

4.4 Capacitive coupling element structure bent in wrist mode

Due to the nature of the wrist mode, the parameters that are altered are different from those used in the previous section for the browsing mode. The bending radius is fixed and the length of the ground plane is altered. In this study, two main properties are examined: firstly, how does bending the ground plane around the wrist affect the η_{tot} (matched antenna elements) and secondly, how does the bending change the Q (unmatched antenna elements). The study is performed using antenna elements CCE#1 (off-ground) and CCE#2 (on-ground), as shown in Fig. 4.1.

For the case with the matched antenna elements, a two-element matching circuit

is used. The component values and circuit topology are determined in the planar case, and the same circuit is then used when the 30 mm bending radius is applied (both with and without the presence of the hand). The component values used with different antenna elements, ground plane lengths and frequencies are given in Tables 4.4–4.5 (component indices refer to their order as seen from the antenna element).

Table 4.4. Component values used to study the bending of the ground plane in the wrist mode. The antenna element is CCE#1 (off-ground). The order of the components (1st and 2nd) refer to their location in the two-element matching circuit as seen from the antenna element.)

l	CCE#1 (off-ground) 920 MHz		CCE#1 (off-ground) 1920 MHz	
[mm]	1st component	2nd component	1st component	2nd component
105	$L_{\text{series}} = 15.9$ nH	$L_{\text{shunt}} = 4.7$ nH	$L_{\text{shunt}} = 1.5$ nH	$C_{\text{series}} = 3.7$ pF
115	$L_{\text{series}} = 16.1$ nH	$L_{\text{shunt}} = 5.5$ nH	$C_{\text{series}} = 74.3$ pF	$L_{\text{shunt}} = 1.9$ nH
125	$L_{\text{series}} = 16.7$ nH	$L_{\text{shunt}} = 5.7$ nH	$C_{\text{series}} = 48.5$ pF	$L_{\text{shunt}} = 2.2$ nH
135	$L_{\text{series}} = 17.4$ nH	$L_{\text{shunt}} = 5.4$ nH	$L_{\text{shunt}} = 2.0$ nH	$C_{\text{series}} = 6.3$ pF
145	$L_{\text{shunt}} = 41.5$ nH	$L_{\text{series}} = 44.4$ nH	$L_{\text{shunt}} = 3.0$ nH	$L_{\text{series}} = 2.5$ nH
155	$L_{\text{shunt}} = 36.8$ nH	$L_{\text{series}} = 52.4$ nH	$L_{\text{shunt}} = 1.7$ nH	$C_{\text{series}} = 2.1$ pF
165	$L_{\text{shunt}} = 16.1$ nH	$C_{\text{series}} = 0.5$ pF	$L_{\text{shunt}} = 1.6$ nH	$C_{\text{series}} = 2.0$ pF
175	$L_{\text{shunt}} = 16.5$ nH	$C_{\text{series}} = 0.4$ pF	$L_{\text{shunt}} = 1.5$ nH	$C_{\text{series}} = 2.5$ pF

Table 4.5. Component values used to study the bending of the ground plane in the wrist mode. The antenna element is CCE#2 (on-ground). The order of the components (1st and 2nd) refer to their location in the two-element matching circuit as seen from the antenna element.

l	CCE#2 (on-ground) 920 MHz		CCE#2 (on-ground) 1920 MHz	
[mm]	1st component	2nd component	1st component	2nd component
105	$L_{\text{shunt}} = 10.2$ nH	$L_{\text{series}} = 19.7$ nH	$C_{\text{shunt}} = 4.8$ pF	$C_{\text{series}} = 3.2$ pF
115	$L_{\text{shunt}} = 11.1$ nH	$L_{\text{series}} = 17.9$ nH	$C_{\text{shunt}} = 4.8$ pF	$C_{\text{series}} = 4.3$ pF
125	$L_{\text{shunt}} = 11.8$ nH	$L_{\text{series}} = 17.9$ nH	$L_{\text{series}} = 0.07$ nH	$C_{\text{shunt}} = 4.7$ pF
135	$L_{\text{shunt}} = 12.1$ nH	$L_{\text{series}} = 19.5$ nH	$L_{\text{series}} = 0.2$ nH	$C_{\text{shunt}} = 4.5$ pF
145	$L_{\text{shunt}} = 11.9$ nH	$L_{\text{series}} = 22.1$ nH	$L_{\text{series}} = 0.2$ nH	$C_{\text{shunt}} = 4.8$ pF
155	$L_{\text{shunt}} = 11.3$ nH	$L_{\text{series}} = 25.9$ nH	$L_{\text{series}} = 0.1$ nH	$C_{\text{shunt}} = 5.3$ pF
165	$L_{\text{series}} = 5.9$ nH	$L_{\text{shunt}} = 2.3$ nH	$L_{\text{series}} = 0.01$ nH	$C_{\text{shunt}} = 5.8$ pF
175	$L_{\text{shunt}} = 6.5$ nH	$C_{\text{series}} = 0.9$ pF	$C_{\text{shunt}} = 5.1$ pF	$C_{\text{series}} = 4.6$ pF

For these ground plane lengths with the 30 mm bending radius, the calculated efficiencies for the CCE#1 (off-ground) and CCE#2 (on-ground) antenna elements are shown in Figs. 4.9 and 4.10, respectively. The index "wrist fs" refers to the case in which the correct bending radius is applied to the ground plane but the hand is not present (free space case).

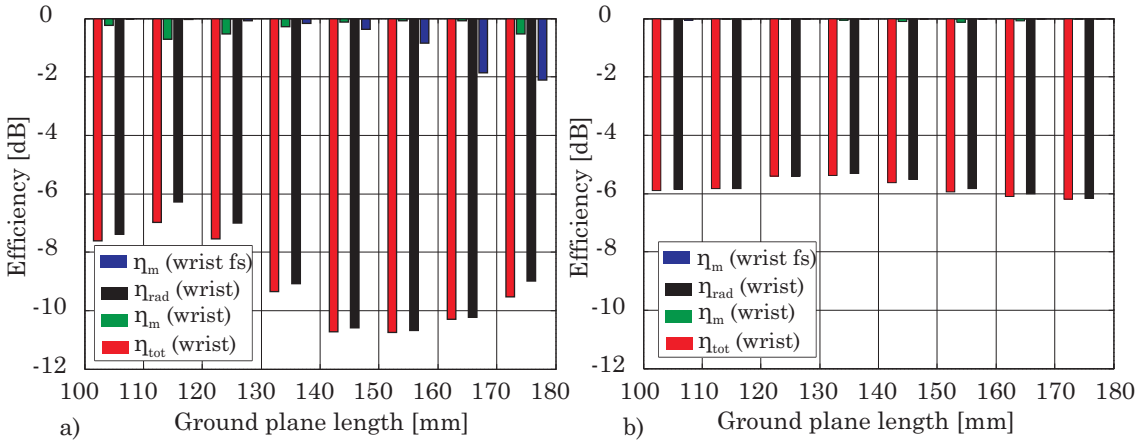

Fig. 4.9. Calculated efficiency in the wrist mode for CCE#1 (off-ground) at a) 920 MHz and b) 1920 MHz frequency.

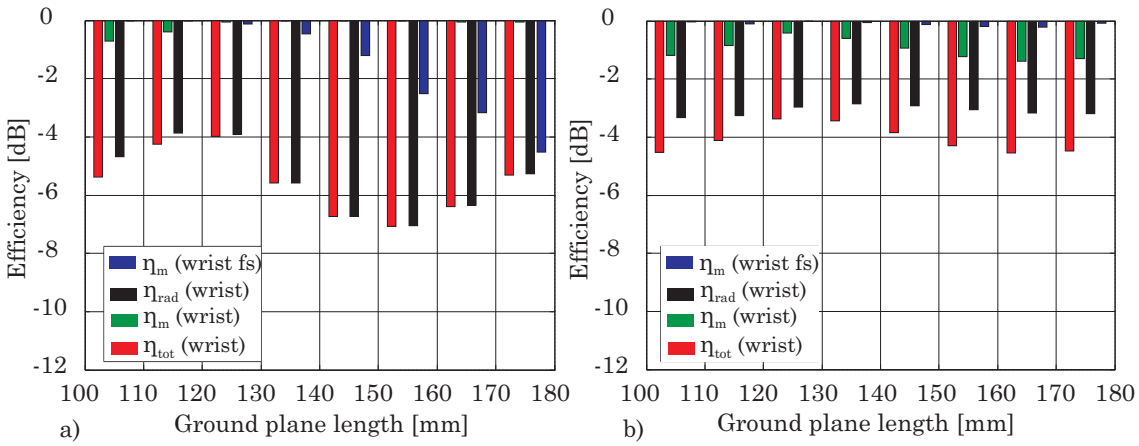

Fig. 4.10. Calculated efficiency in the wrist mode for CCE#2 (on-ground) at a) 920 MHz and b) 1920 MHz frequency.

From the diagrams of Figs. 4.9–4.10 it can be seen that at the lower frequency, both antenna elements show an increasing frequency detuning (meaning decreasing η_{m}) in the free space case beyond 135 mm ground plane length. This effect is stronger with the CCE#2 (on-ground) element. When looking at the same cases when the hand is present, it is clear that the η_{m} is significantly improved. This improvement is most likely due to an improved matching level at the 920 MHz frequency rather than reduced frequency detuning. Studies on the effect of the user in conventional mobile devices have shown that the properties of the human tissue (especially the

permittivity) cause additional frequency shift and that the hand usually shifts the resonance downwards [10, 55]. At the 1920 MHz frequency, changes in the η_{m} are smaller than at 920 MHz.

The decreasing η_{tot} is mainly due to the absorption of the power into the hand (reduced η_{rad}). At the higher frequency, the frequency detuning is extremely small, both in free space and when the hand is applied, with all lengths of the ground plane and for both antenna elements considered. The reason for this is that at higher frequencies, the contribution of the ground plane to the overall radiation performance of the antenna structure reduces. Therefore, when the antenna element (which remains largely unchanged in the bending) begins to act as the principal radiator, it is expected that the difference in the η_{m} should be fairly small.

The cases in which the performance of the antenna is least affected by the bending and the presence of the hand can be determined by looking at the η_{tot}. At the 920 MHz frequency, both antenna elements studied have the best η_{tot} with the 115–125 mm ground plane lengths, whereas at 1920 MHz, the best η_{tot} is with 125–135 mm ground plane lengths. However, with the CCE#1 (off-ground) antenna element at 1920 MHz, the variation between the η_{tot} with the different ground plane sizes is smaller than in the other three cases. This is most likely due to a smaller change in the Q_{el} for the CCE#1 (off-ground) element (see Fig. 4.11), especially if it is assumed that the Q_{gp} remains fairly unchanged.

In the case of Figs. 4.9–4.10, the antenna elements are matched, which means that also the circuit topology used can have an effect on the results. For this reason, the performance of the antenna structures is also observed through the calculated Q_{z}, in which no matching circuit is used. The effect of the ground plane length on the Q_{z} in the wrist mode is illustrated in Fig. 4.11 at 920 MHz and 1920 MHz frequencies. As was the case in Figs. 4.9–4.10, the index ”wrist fs” refers to the bent case without the hand (free space case). In the ”wrist fs” case, only the matching efficiency is shown. This is due to the fact that the entire antenna structure is modelled as PEC, which means that the radiation efficiency is 1 (0 dB). Therefore, the matching efficiency can be used as a measure of the (total) efficiency of the antenna structure, as can be concluded from Eq. (2.15), which can be written in dBs as $\eta_{\mathrm{tot}}\,[\mathrm{dB}] = \eta_{\mathrm{rad}}\,[\mathrm{dB}] + \eta_{\mathrm{m}}\,[\mathrm{dB}]$.

From the curves of Fig. 4.11 it is possible to see that especially at 920 MHz, the general behaviour of the Q_{z} is fairly similar in the planar and ”wrist fs” cases (with all ground plane lengths and both antenna elements). Because the ground planes used are the same for both cases, the observable differences are likely caused by the differences in the antenna elements and their Q. In principle, the overall Q has a contribution from both the ground plane and the antenna element, as given by

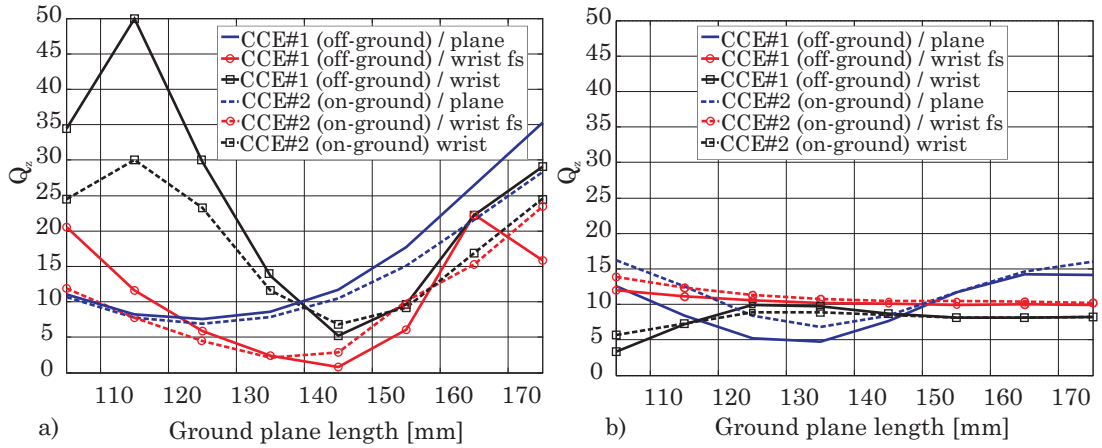

Fig. 4.11. Calculated Q_z in the wrist mode at a) 920 MHz and b) 1920 MHz frequency.

$1/Q_{tot} \propto 1/Q_{el} + 1/Q_{gp}$, but for reasons to be discussed in Section 4.5.1, the two sides of this expression are not equal. With a given ground plane length, the Q_{gp} is the same for both on- and off-ground positioned antenna elements.

The curves of Fig. 4.11 also show that in the planar case, the difference between the Q_z of the two antenna elements is larger with longer ground plane lengths at 920 MHz, and at 1920 MHz, this difference is larger with the shorter ground plane lengths. At the lower frequency, the Q_z of the CCE#1 (off-ground) element is larger than that of the CCE#2 (on-ground) element, whereas at the higher frequency, the behaviour is opposite. These observations, as well as the significantly larger variation of the Q_z at 920 MHz frequency, are all in agreement with the larger contribution of the ground plane to the radiation at the lower frequencies.

When observing the behaviour of both antenna elements at 920 MHz, it can be seen that the Q_z has its minimum at around 145 mm ground plane length (the number of ground plane lengths is too small so as to give an exact value). This region correspond to that with the lowest radiation efficiency (as seen in Figs. 4.9–4.10). One of the reasons behind this effect is the power that is absorbed into the hand and thus not radiated (absorption loss due to conductivity), but also the changes in the operating mode of the antenna structure (the antenna begins to operate more in the magnetic mode rather than in the electric mode).

At the lower frequency, there is a sharp increase in the Q_z with ground plane lengths between 115 and 145 mm. The hand causes additional losses (seen as a decrease in η_{rad} in Figs. 4.9–4.10), which according to, e.g., Eq. (2.5) should cause a decrease in the Q_z. However, the effect of the hand is twofold, due to the two key parameters, namely conductivity and permittivity. The frequency detuning that may be seen in the presence of the user is caused by the permittivity. In the case of the bent structures, the sharp increase in Q_z can be associated with the permittivity

causing an increase in electric energy stored in the near field, which can be seen, e.g., as rotation of the impedance on the Smith chart. The increasing stored energy can compensate for the increasing losses, and in some cases also exceed them, thereby resulting in the increasing Q_{z} seen in Fig. 4.11.

As was discussed in Section 2.2.2, the reactive energy stored in the near fields of the antenna structure can be categorised into electric (capacitive) and magnetic (inductive) energy. Of these two types of energy modes, the capacitive coupling element antennas used in this work utilise mostly the electric one because its electric dipole moment is considerably larger than the magnetic dipole moment. When the ground plane is bent around the wrist, the energy stored in the non-radiating magnetic mode increases, thereby decreasing the radiation efficiency. With tighter bending, the shape of the antenna structure also resembles more and more that of a loop antenna, in which the magnetic dipole moment dominates. A longer ground plane, covers a larger section of the wrist, and hence also the contribution of the magnetic mode increases.

4.5 Modelling of ground plane bending with equivalent circuit

The results presented in the previous sections show some of the effects that changing the shape of the ground plane can have on the performance of the antenna elements. So far, the results have offered an insight into *what* happens when the shape of the ground plane is bent, and also some explanations as to what could be the reason behind these changes. Of these two questions, the more interesting and important one is *why* do the changes observed actually take place, i.e. what is the underlying physics.

One way of attempting to further answer the second question is to use the resonator-based equivalent circuit model discussed in Section 2.3 (see Fig. 2.5). In this model, the series and parallel resonators model the antenna element and the different resonant wavemodes of the ground plane, respectively, and they describe the performance of the combined antenna and ground plane structure (in the unbent case). In order to take into account the effects of the bending, the topology of the equivalent circuit for the planar case has to be suitably modified, either by changing the values of individual components or by placing some additional components into the circuit.

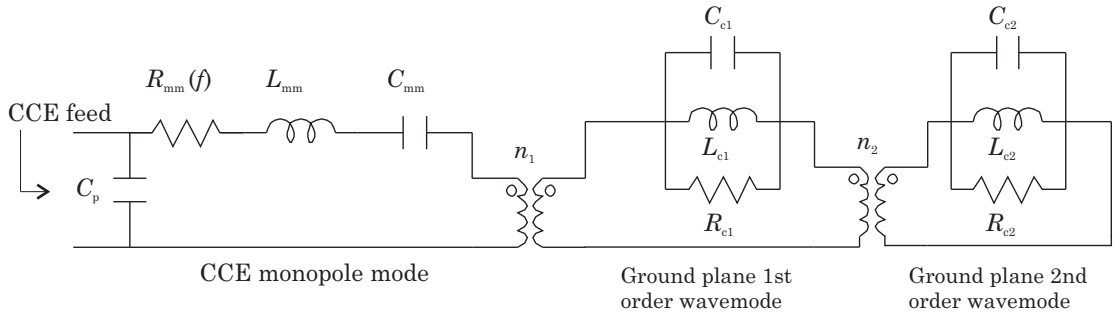

Fig. 4.12. Circuit topology for the equivalent circuit with the CCE monopole mode and the two lowest-order ground plane wavemodes.

4.5.1 Equivalent circuit for the planar case

The starting point with the equivalent circuit is to decide the number of wavemodes that are to be considered in the model. The number of wavemodes defines the number of resonators in the circuit, and consequently also the frequency range in which the model is valid. With a larger number of resonators, the complexity of the model increases, but the equivalent circuit can also be used for a wider range of frequencies.

In this work, the purpose is to improve the understanding of the effects and changes that are associated with the bending of the ground plane. As can be seen, e.g., in Fig. 3.6, the most interesting changes are occurring below 3 GHz, and for this reason, the frequency range to be covered with the circuit model is from 0.5 GHz to 3 GHz. This range can be achieved by using three resonators: one for the so-called monopole mode of the coupling element, and individual resonators for the first and second wavemodes, respectively, of the ground plane.

The basic circuit topology for the planar case is shown in Fig. 4.12, and it is for the case of CCE#2 (on-ground) placed at the end of the 105 mm ground plane. An on-ground element is chosen because the basic circuit topology shown in, e.g., Fig. 2.5 and [44] is valid at least for this element position. It is possible that the monopole mode of an off-ground positioned antenna element requires slightly different circuitry, or that it may be more challenging to determine the Q_{el} in this case. The component values for the resonators are derived based on the impedance of the structure simulated using SEMCAD, as well as on the formulas for the Q of RLC components given in Section 2.3.1.

The maximum Q_0 of the CCE#2 (on-ground) antenna element was found with the ground plane length of 20 mm ($Q_{\mathrm{mm}} \approx 72$), and the resonant frequency of the monopole mode is $f_{\mathrm{r,mm}} = 1.54\,\mathrm{GHz}$. When the Q is the largest, the ground plane does not in principle radiate at all (the source of the radiation is the antenna element), as was discussed in Section 2.3.1. The resonant frequencies of the first and second order

ground plane wavemodes are $f_{\mathrm{r,c1}} = 1.12\,\mathrm{GHz}$ and $f_{\mathrm{r,c2}} = 2.37\,\mathrm{GHz}$, respectively. The component values for the equivalent circuit in the planar case that are calculated with Eqs. (2.17)–(2.19) are shown in Table 4.6.

The Q_{r} of the ground plane wavemodes is needed to determine the component values for the corresponding resonators, and in order to obtain the correct values for the 50 x 105 mm^2 ground plane, the associated eigenvalue problem based on the characteristic wavemode theory would have to be solved. Even though the antenna element and the ground plane have Q:s that can be determined separately, it is not possible to obtain either Q_{el} or Q_{gp} from the expression $1/Q_{\mathrm{tot}} = 1/Q_{\mathrm{el}} + 1/Q_{\mathrm{gp}}$ which has a form similar to, e.g., Eq. (2.11). This is due to the fact that this kind of relationship cannot be used when the coupled resonators are different, as is the case with the combined antenna element and ground plane structure. The reason is that the different (i.e. dissimilar) resonators have different resonant frequencies and amounts of stored energy, which means that they cannot be reduced from $Q = \omega W/P$ type expressions. Hence, the way to overcome this issue is to use the previously discussed characteristic wavemode theory.

However, performing the calculations was not feasible in the time frame of this master's thesis, and so the initial components are calculated using Q_{r} values reported in [48] for a 40 x 100 mm^2 ground plane (the actual values for the 50 x 105 mm^2 ground plane are probably fairly close to those of [48]). The initial radiation resistances are determined from the simulated resistance of the overall antenna structure, and their values are $R_{\mathrm{c1}} = 7.3\,\Omega$ and $R_{\mathrm{c2}} = 6.5\,\Omega$, respectively, for the first and second order wavemodes of the ground plane, respectively.

Table 4.6. Calculated component values used with the equivalent circuit shown in Fig. 4.12.

Wavemode	L [nH]	C [pF]	R [Ω]	f_{r} [GHz]	Q	Other components
Monopole	4.5	2.38	0.6	1.54	72	$C_{\mathrm{p}} = 0.24$ pF
Ground plane 1st order	1.25	16.1	7.3	1.12	2.3	$n_1 = 1$
Ground plane 2nd order	0.17	27.3	6.5	2.37	3.0	$n_2 = 1$

In order to improve the agreement between the simulated results and those given by the circuit model, the component values had to be slightly tuned. This tuning takes into account effects such as the small change in the resonant frequencies of the ground plane wavemodes when the antenna element is also included in the structure [76]. However, the tuning does not change the basic circuit topology, and the final component values used are given in Table 4.7. The resistance, reactance and

reflection coefficient at the feed given by this circuit model are depicted in Fig. 4.13, in which the results are also compared to those given by the simulations.

The results shown in Fig. 4.13 show that a good agreement between the simulation results and the results given by the equivalent circuit can be obtained. At frequencies above 2.5 GHz, the reflection coefficient results begin to show some more significant deviation, the source of which is the difference between the simulated and modelled reactance curves (the resistance is modelled with very good accuracy over the entire frequency range).

Table 4.7. Final component values for the equivalent circuit shown in Fig. 4.12.

Wavemode	L [nH]	C [pF]	R [Ω]	f_r [GHz]	Q	Other components
Monopole	4.5	2.38	0.6	1.54	72	$C_p = 0.32\,\text{pF}$
Ground plane 1st order	0.85	25.7	12.3	1.08	N/A	$n_1 = 0.82$
Ground plane 2nd order	0.26	16.1	7.54	2.46	N/A	$n_2 = 0.88$

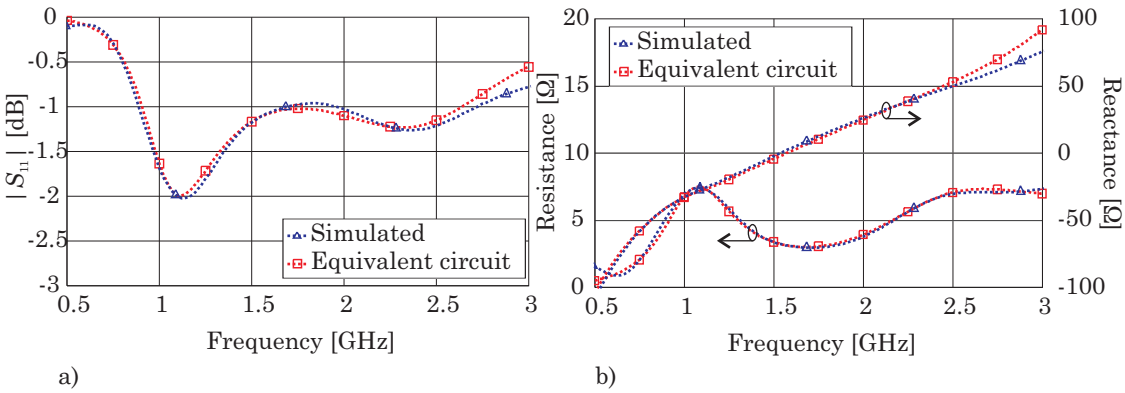

Fig. 4.13. Comparison between the simulation results and those given by the equivalent circuit of Fig. 4.12: a) $|S_{11}|$ curves, and b) resistance and reactance.

4.5.2 Modelling of ground plane bending in free space

As can be seen, the circuit model that is derived for the planar case is able to provide an accurate description of the impedance properties of the CCE structure (both for resistance and reactance), as well as for the overall input reflection coefficient ($|S_{11}|$). Fig. 4.14 shows how the behaviour of the unmatched $|S_{11}|$ curve changes when a bending radius of 20 mm is applied (see Fig. 4.2). Both a Cartesian plot and the Smith chart view are shown. The 20 mm radius is chosen because with the 105 mm ground plane length, it represents the most extreme bending case. It is therefore possible to assume that the changes in the performance due to the bending are the

largest in this case.

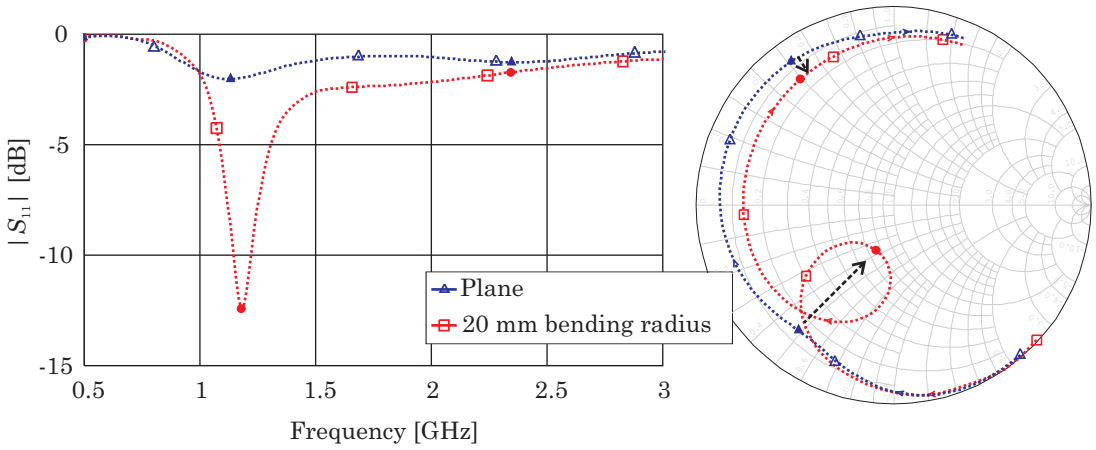

Fig. 4.14. Changes in the $|S_{11}|$ curves when the bending radius of 20 mm is applied to the ground plane of the CCE#2 (on-ground) structure.

The curves shown in Fig. 4.14 show that the bending causes changes in the resonant frequencies and the matching level of the ground plane wavemodes, as well as on the coupling to the wavemodes. On the Smith chart it can be seen that the coupling to the first ground plane wavemode increases (the curve and the loop generated shift closer to the centre of the Smith chart), and at the second order wavemode the coupling also slightly increases (the curve is shifted closer to the centre).

In order to model the response of the bent structure, the circuit topology of Fig. 4.12 has to be suitably modified. The changes in the resonant frequencies can be modelled by placing additional reactive elements (inductance and capacitance) to the resonators of the ground plane wavemodes. Like all other components and parameters in the equivalent circuit, also these components and their values have physical meaning to justify their presence in the model. The coupling to the different wavemodes can be altered through the winding ratio of the transformers. The additional resistance placed in the resonator of the second ground plane wavemode helps to reduce the overall radiation resistance of this wavemode because R_{c2} is parallel to $R_{\mathrm{c2,b}}$.

Apart from the winding ratio of the transformers, the component values of the basic circuit topology for the planar case are kept the same. This approach enables a more clear insight into the physical effects of the bending. One additional benefit is that the changes to the circuit are easier to visualise. The component values of the monopole mode are kept the same because the antenna element is not significantly altered when bending the ground plane. With decreasing bending radius, the distance between the ground plane and the antenna element (just below the element) actually begins to increase slightly due to the curvature of the ground plane. This

slight increase results in a minor increase of the volume of the antenna, which can cause a small decrease in the Q_{el}. However, the effect of this change is most likely very insignificant.

The modified circuit topology is shown in Fig. 4.15, and the additional or modified component values are given in Table 4.8. A comparison between the response given by this circuit and simulation results is shown in Fig. 4.16.

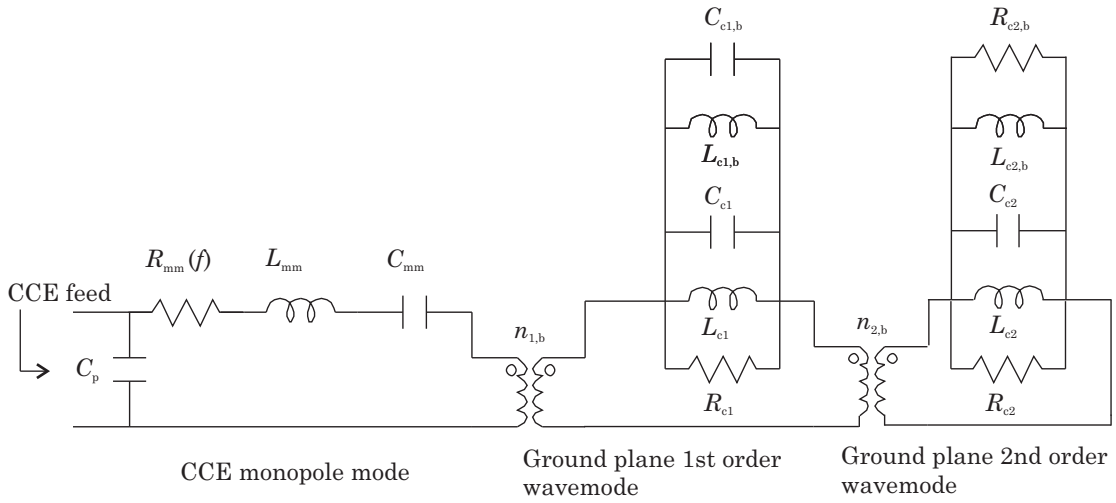

Fig. 4.15. Equivalent circuit model for the case in which the 20 mm bending radius is used. Additional or modified components are identified with the subscript b.

Table 4.8. Component values for the additional or modified components in Fig. 4.12 that are introduced in order to take into account the changes caused by the bending.

Wavemode	Component 1	Component 2	Component 3	Other components
Monopole	–	–	–	–
Ground plane 1st order	$L_{c1,b} = 0.56$ nH	$C_{c1,b} = 24.9$ pF	–	$n_{1,b} = 1.82$
Ground plane 2nd order	$L_{c2,b} = 1.14$ nH	$R_{c2,b} = 3.28\ \Omega$	–	$n_{2,b} = 0.76$

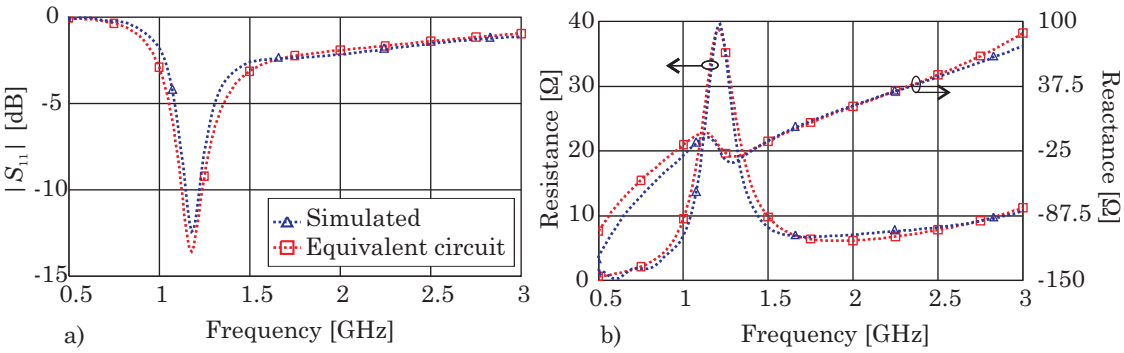

Fig. 4.16. Comparison between the simulation results and those given by the equivalent circuit of Fig. 4.15: a) $|S_{11}|$ curves and b) resistance and reactance.

As can be seen, the behaviour of the bent antenna structure can be modelled quite accurately with the help of the additional resistive and reactive elements as well as altered transformer winding ratios. The increasing resistance level as well as the dip in the reactance at the first ground plane wavemode can be traced very accurately. The slight differences that remain between the simulation and circuit model results can partially be caused by the discrepancies in the initial seed values that were used. Furthermore, it has been assumed in the circuit model that the Q of the ground plane wavemodes is the same for both the planar and bent ground planes, which may in reality not be the case. This assumption was made due to a lack of feasible methods to validate this claim.

The circuit model that has been used in this section to model the effects of the bending, including type, location and values of the additional components, has been derived for a single bending case (20 mm bending radius, 105 mm ground plane). With a different bending radius, the component values are bound to change, but the circuit topology used in the modified case can be regarded as fairly general. In some cases, it may be necessary to include additional capacitance and/or resistance into all resonators of the ground plane wavemodes, but the physical interpretation of these components is similar to the ones that have been analysed here.

5. Summary and conclusions

In this master's thesis, the performance of antennas in bendable mobile devices have been studied. The two ground plane sizes (50 x 105 and 50 x 175 mm^2) as well as the type of antenna element (CCE, capacitive coupling element) that have been used are typical for current mobile terminals, and may also find novel applications in future devices. The two main objectives of this work are to firstly observe what kind of changes can be seen in different quantities when the shape of the ground plane is no longer planar. The second main objective is to understand why the different changes take place.

The problem at hand is analysed using computer simulations and a resonator-based equivalent circuit model. From the computer simulations (using both electromagnetic and circuit simulators) it is clear that CCE antenna structures are most affected by the bending around the resonant frequencies of the ground plane. Both the resonant frequencies of and coupling to the ground plane wavemodes change when the bending radius is varied. With the CCE, it is possible to observe the effect of the bending on the individual wavemodes particularly when the non-resonant antenna element is not matched to any particular frequency with an external matching circuit.

When the mobile terminal is bent in the presence of the hand, the bending reduces the absorption of the power into the hands in some cases (in the so-called browsing mode). This effect is caused by the changes in the current distributions of the ground plane wavemodes when the bending is applied. In the wrist mode, certain antenna elements and ground plane lengths cause an increase in the quality factor calculated from the input impedance (Q_{z}), even though the hand introduces additional losses that should in principle reduce the Q_{z}. The increase may be caused by additional energy storage due to the properties of the hand. However, further studies on this subject are still needed to better understand the actual mechanism behind this behaviour.

By using a resonator-based equivalent circuit model it is possible to obtain a better physical understanding of the reasons behind the changes that take place when the ground plane is bent. The different resonators in the model correspond to the individual resonant wavemodes of the ground plane, to which the CCE couples. The results

from the equivalent circuit show that the bending changes the resonant frequencies of the ground plane wavemodes as well as the coupling from the antenna element to these wavemodes. Both these changes can be modelled with the circuit model by using a proper circuit topology, including additional circuit elements and modified component values.

Future work on the subject could include the study of different ground plane sizes and improved modelling of the bent ground plane. Of the former, both smaller and larger ground planes (in terms of both length and width) can be considered in order to find dimensions that are the most (or least) sensitive to bending. From the results obtained in this thesis, it is possible to assume that the antenna element remains fairly unchanged in the bending. This means that a more accurate model of the effect of the bending on the ground plane, e.g., through characteristic wavemode theory, could provide further insight into the problem at hand. This modelling could also be done in the presence of the user, in which case the equivalent circuit model based approach may also provide an improved understanding to some of the phenomena observed in this work when the hand is present.

As most of the results of this master's thesis have been obtained using computer simulations, the future work on this subject also includes the validation of the simulated results by means of measurements. These measurements can be performed both in free space and in the presence of the user.

Bibliography

[1] P. Vainikainen, J. Holopainen, C. Icheln, O. Kivekäs, M. Kyrö, M. Mustonen, S. Ranvier, R. Valkonen, and J. Villanen, ”More than 20 antenna elements in future mobile phones, threat or opportunity?,” *Proceedings of the 3rd European Conference on Antennas and Propagation (EuCAP 2009)*, Berlin, Germany, Mar. 2009, pp. 2940–2943.

[2] Nokia Lumia 920 specifications, [online], http://www.nokia.com/global/products/phone/lumia920/specifications (Cited Nov. 30, 2012).

[3] K. R. Boyle, Y. Yuan, and L. P. Ligthart, ”Analysis of mobile phone antenna impedance variations with user proximity,” *IEEE Transactions on Antennas and Propagation*, vol. 55, no. 2, pp. 364–372, Feb. 2007.

[4] R. Valkonen, J. Ilvonen, K. Rasilainen, J. Holopainen, C. Icheln, and P. Vainikainen, ”Avoiding the interaction between hand and capacitive coupling element based mobile terminal antenna,” *5th European Conference on Antennas and Propagation (EuCAP 2011)*, Rome, Italy, Apr. 2011, pp. 2781–2785.

[5] M. Pelosi, O. Franek, M. Bergholz Knudsen, and G. Frølund Pedersen, ”User’s proximity effects in mobile phones,” *Proceedings of the 3rd European Conference on Antennas and Propagation (EuCAP 2009)*, Berlin, Germany, Mar. 2009, pp. 1022-1024.

[6] M. Pelosi, O. Franek, G. Frølund Pedersen, and M. Bergholz Knudsen, ”User’s impact on PIFA antennas in mobile phones,” *IEEE 69th Vehicular Technology Conference (VTC-Spring 2009)*, Barcelona, Spain, Apr. 2009.

[7] J. Krogerus, J. Toivanen, C. Icheln, and P. Vainikainen, ”Effect of the human body on total radiated power and the 3-D radiation pattern of mobile handsets,” *IEEE Transactions on Instrumentation and Measurements*, vol. 56, no. 6, pp. 2375–2385, Dec. 2007.

[8] A. A. H. Azremi, J. Ilvonen, R. Valkonen, J. Holopainen, O. Kivekäs, C. Icheln, and P. Vainikainen, ”Performance analysis of broadband coupling-element-based

multiantenna structure for mobile terminal with hand effects," *21st Annual IEEE International Symposium on Personal, Indoor and Mobile Radio Communications (PIMRC)*, Istanbul, Turkey, Sep. 2010, pp. 1110–1115.

[9] R. Valkonen, S. Myllymäki, A. Huttunen, J. Holopainen, J. Ilvonen, P. Vainikainen, and H. Jantunen, "Compensation of finger effect on a mobile terminal antenna by antenna selection," *2010 International Conference on Electromagnetics in Advanced Applications (ICEAA)*, Cape Town, South Africa, Sep. 2010, pp. 364–367.

[10] J. Ilvonen, J. Holopainen, O. Kivekäs, R. Valkonen, C. Icheln, and P. Vainikainen, "Balanced antenna structures for mobile terminals," *Proceedings of the 4th European Conference on Antennas and Propagation (EuCAP 2010)*, Barcelona, Spain, Apr. 2010.

[11] M. Berg, M. Sonkki, and E. T. Salonen, "Absorption loss reduction in a mobile terminal with switchable monopole antennas," *IEEE Transactions on Antennas and Propagation*, vol. 59, no. 11, pp. 4379–4383, Nov. 2011.

[12] T. Kellomäki, *Effects of the Human Body on Single-Layer Wearable Antennas*, Doctoral Thesis, Tampere University of Technology, Publication 1025, 2012.

[13] E. K. Kaivanto, M. Berg, E. Salonen, and P. de Maagt, "Wearable circularly polarized antenna for personal satellite communication and navigation," *IEEE Transactions on Antennas and Propagation*, vol. 59, no. 12, pp. 4490–4496, Dec. 2011.

[14] M. Mikkola, *Effect of Complex Handset Structures on Handset Antenna Perfomance*, Master's Thesis, Helsinki University of Technology, Oct. 2005.

[15] J. Villanen, M. Mikkola, C. Icheln, and P. Vainikainen, "Radiation characteristics of antenna structures in clamshell-type phones in wide frequency range," *IEEE 65th Vehicular Technology Conference (VTC2007-spring)*, Dublin, Ireland, Apr. 2007, pp. 382–386.

[16] Nokia Morph Concept, [online], http://research.nokia.com/morph (Cited Nov. 30, 2012).

[17] Nokia Twist Concept, [online], http://technabob.com/blog/2011/11/09/nokia-twist-concept-phone (Cited Nov. 30, 2012).

[18] Nokia 888 Concept Phone, [online], http://www.conceptmobiles.com/nokia-communicator-888-concept (Cited Nov. 30, 2012).

[19] Special Issue on Flexible Electronics Technology, Part 1: Systems and Applications, *Proceedings of the IEEE*, vol. 93, no. 7, Jul. 2005.

[20] Special Issue on Flexible Electronics Technology, Part 2: Materials and Devices, *Proceedings of the IEEE*, vol. 93, no. 8, Aug. 2005.

[21] B. R. Chalamala and D. Temple, "Big & bendable [flexible plastic-based circuits]," *IEEE Spectrum*, vol. 42, no. 9, pp. 50–56, Sep. 2005.

[22] K. J. Allen, "Reel to real: prospects for flexible displays," *Proceedings of the IEEE*, vol. 93, no. 8, pp. 1394–1399, Aug. 2005.

[23] I. Lindell and K. Nikoskinen, *Antenniteoria* (in Finnish), Otatieto, 3rd ed., 1995.

[24] H. A. Wheeler, "The radiansphere around a small antenna," *Proceedings of the IRE*, vol. 47, no. 8, pp. 1325–1331, Aug. 1959.

[25] IEEE Std 145-1993, IEEE Standard Definition of Terms for Antennas. IEEE, 1993, 40 p.

[26] R. C. Hansen, "Fundamental limitations in antennas," *Proceedings of the IEEE*, vol. 69, no. 2, pp. 170–182, Feb. 1981.

[27] J. Villanen, J. Ollikainen, O. Kivekäs, and P. Vainikainen, "Coupling element based mobile terminal antenna structures," *IEEE Transactions on Antennas and Propagation*, vol. 54, no. 7, pp. 2142–2153, Jul. 2006.

[28] V. Kaajakari, A. Alastalo, K. Jaakkola, and H. Seppä, "Variable antenna load for transmitter efficiency improvement," *IEEE Transactions on Microwave Theory and Techniques*, vol. 55, no. 8, pp. 1666–1672, Aug. 2007.

[29] J. D. Kraus and R. J. Marhefka, *Antennas for All Applications*, John Wiley & Sons, 3rd ed., 2002.

[30] J. Ollikainen, *Design and Implementation Techniques of Wideband Mobile Communications Antennas*, Doctoral Thesis, Helsinki University of Technology, Radio Laboratory, Nov. 2004.

[31] A. Räisänen and A. Lehto, *Radiotekniikan perusteet* (in Finnish), Otatieto, 12th ed., 2007.

[32] H. F. Pues and A. R. van de Capelle, "An impedance-matching technique for increasing the bandwidth of microstrip antennas," *IEEE Transactions on Antennas and Propagation*, vol. 37, no. 11, pp. 1345–1354, Nov. 1989.

[33] J. Rahola, ”Bandwidth potential and electromagnetic isolation: tools for analysing the impedance behaviour of antenna systems,” *Proceedings of the 3rd European Conference on Antennas and Propagation (EuCAP 2009)*, Berlin, Germany, Mar. 2009, pp. 944–948.

[34] H. W. Bode, *Network Analysis and Feedback Amplifier Design*, D. Van Nostrand Company, Inc., 5th printing, Apr. 1949.

[35] R. M. Fano, ”Theoretical limitations on the broadband matching of arbitrary impedances,” Technical Report no. 41, Research Laboratory of Electronics, MIT, Jan. 1948.

[36] E. Nyfors and P. Vainikainen, *Industrial Microwave Sensors*, Artec House, 1989.

[37] R. Vaughan and J. Bach Andersen, *Channels, Propagation and Antennas for Mobile Communications*, The IEE Electromagnetic Waves Series 50, 2003.

[38] A. D. Yaghjian and S. R. Best, ”Impedance, bandwidth and Q of antennas,” *IEEE Transactions on Antennas and Propagation*, vol. 53, no. 4, pp. 1298–1324, Apr. 2005.

[39] L. J. Chu, ”Physical limitations of omni-directional antennas,” *Journal of Applied Physics*, vol. 19, Dec. 1948, pp. 1163–1175.

[40] J. S. McLean, ”A re-examination of the fundamental limits on the radiation Q of electrically small antennas,” *IEEE Transactions on Antennas and Propagation*, vol. 44, no. 5, pp. 672–676, May 1996.

[41] R. Valkonen, J. Ilvonen, and P. Vainikainen, ”Naturally non-selective handset antennas with good robustness against impedance mistuning,” *Proceedings of the 6th European Conference on Antennas and Propagation (EuCAP 2012)*, Prague, Czech Republic, Mar. 2012, pp. 796–800.

[42] J. Ilvonen, R. Valkonen, J. Holopainen, O. Kivekäs, and P. Vainikainen, ”Reducing the interaction between user and mobile terminal antenna based on antenna shielding,” *Proceedings of the 6th European Conference on Antennas and Propagation (EuCAP 2012)*, Prague, Czech Republic, Mar. 2012, pp. 1889–1893.

[43] P. Vainikainen, J. Ollikainen, O. Kivekäs, and I. Kelander, ”Resonator-based analysis of the combination of mobile handset antenna and chassis,” *IEEE Transactions on Antennas and Propagation*, vol. 50, no. 10, pp. 1433–1444, Oct. 2002.

[44] J. Holopainen, R. Valkonen, O. Kivekäs, J. Ilvonen, and P. Vainikainen, ”Broadband equivalent circuit model for capacitive coupling element-based mobile terminal antenna,” *IEEE Antennas and Wireless Propagation Letters*, vol. 6, pp. 716–719, 2010.

[45] K. Fujimoto, A. Henderson, A. Hirasawa, and J. R. James, *Small Antennas*, Research Studies Press, 1987.

[46] D. M. Pozar, *Microwave Engineering*, John Wiley & Sons, 4th ed., 2012.

[47] T. Taga, ”Analysis of planar inverted-F antennas and antenna design for portable radio equipment,” in *Analysis, Design and Measurement of Small and Low-Profile Antennas*, K. Hirasawa and M. Haneishi (editors), Artec House, 1992, Chapter 5, pp. 161–180.

[48] C. T. Famdie, W. L. Schroeder, and K. Solbach, ”Numerical analysis of characteristic modes on the chassis of mobile phones,” *Proceedings of the 1st European Conference on Antennas and Propagation (EuCAP 2006*, Nice, France, Nov. 2006, pp. 358–361.

[49] J. Holopainen, R. Valkonen, O. Kivekäs, J. Ilvonen, L. Martínez, P. Vainikainen, J. R. Kelly, and P. S. Hall, ”Equivalent circuit model-based approach on the user body effect of a mobile terminal antenna,” *2010 Loughborough Antennas & Propagation Conference*, Loughborough, UK, Nov. 2010, pp. 217–220.

[50] R. J. Garbacz, *A Generalized Expansion for Radiated and Scattered Fields*, Doctoral Thesis, Ohio State University, Columbus, OH., USA, 1968.

[51] R. F. Harrington and J. R. Mautz, ”Theory of characteristic modes for conducting bodies,” *IEEE Transactions on Antennas and Propagation*, vol. 19, no. 5, pp. 622–628, Sep. 1971.

[52] M. Sonkki, E. Antoninu, M. Ferrando, and E. Salonen, ”Small radiating ground plane with higher order modes,” *Proceedings of the 5th European Conference on Antennas and Propagation (EuCAP 2011)*, Rome, Italy, Apr. 2011, pp. 1243–1247.

[53] M. Cabedo-Fabrés, E. Antonino-Daviu, A. Valero-Nogueira, and M. Ferrando-Bataller, ”The theory of characteristic modes revisited: a contribution to the design of antennas for modern applications,” *IEEE Antennas and Propagation Magazine*, vol. 49, no. 5, pp. 52–68, Oct. 2007.

[54] P. Hui, ”Positive hand effects on mobile handset antennas,” *Asia-Pacific Microwave Conference (APMC 2008)*, Macau, China, Dec. 2008.

[55] J. Holopainen, J. Poutanen, C. Icheln and P. Vainikainen, ”User effect of antennas for handheld DVB-H terminals,” *International Conference on Electromagnetics in Advanced Applications (ICEAA 2007)*, Turin, Italy, Sep. 2007, pp. 496–499.

[56] J. Wiart, R. Mittra, ”Power deposited in biological tissues from a hand-held mobile antenna,” *Antennas and Propagation Society International Symposium (APS)*, 1996 Digest, vol. 2, Jul. 1996, pp. 1104–1107.

[57] A. Lehtola *et al*., Lecture notes of the course ”Radio Systems in Telecommunications II,” Aalto University, School of Electrical Engineering, Apr. 2012.

[58] T. Huang and K. R. Boyle, ”User interaction studies on handset antennas,” *The 2nd European Conference on Antennas and Propagation (EuCAP 2007)*, Edinburgh, Scotland, Nov. 2007.

[59] M. Pelosi, O. Franek, M. Bergholz Knudsen, M. Christensen, and G. Frølund Pedersen, ”A grip study for talk and data modes in mobile phones,” *IEEE Transactions on Antennas and Propagation*, vol. 57, no. 4, pp. 856–865, Apr. 2009.

[60] C. C. Johnson and A. W. Guy, ”Nonionizing electromagnetic wave effects in biological materials and systems,” *Proceedings of the IEEE*, vol. 60, no. 6, pp. 692–718, Jun. 1972.

[61] IEEE Std 1528-2003 IEEE Recommended Practice for Determining the peak Spatial-Average Specific Absorption Rate (SAR) in the Human Head from Wireless Communications Devices: Measurement Techniques, 149 p., 2003.

[62] Q. Balzano, J. Irwin, and R. Steel, ”Investigation of the impedance variation and radiation loss in portable radios,” *IEEE Antennas and Propagation Society International Symposium*, vol. 13, Jun. 1975, pp. 89–92.

[63] P. Ramachandran, Z. D. Milosavljevic, and C. Beckmann, ”Adaptive matching circuitry for compensation of finger effect on handset antennas,” *Proceedings of the 3rd European Conference on Antennas and Propagation (EuCAP 2009)*, Berlin, Germany, Mar. 2009, pp. 801–804.

[64] SEMCAD-X, an FDTD-based electromagnetic simulator, ver. 14.8 Aletsch, Schmid & Partner Engineering AG, Zurich, Switzerland. [Online]. Available: http://www.semcad.com (Cited Nov. 30, 2012).

[65] HFSS, an FEM-based electromagnetic simulator, ver. 13.0, ANSYS, Canonsburg, PA, USA. [Online]. Available: http://www.ansys.com (Cited Nov. 30, 2012).

[66] CST Microwave Studio, an FDTD/FIT-based electromagnetic simulator, ver. 2010, CST AG, Darmstadt, Germany. [Online]. Available: http://www.cst.com (Cited Nov. 30, 2012).

[67] IE3D, a MoM-based electromagnetic simulator, ver. 15.10, Mentor Graphics, Wilsonville, OR., USA. [Online]. Available: http://www.mentor.com (Cited Nov. 30, 2012).

[68] C. Icheln, J. Ollikainen, and P. Vainikainen, ”Reducing the influence of feed cables on small antenna measurements,” *Electronics Letters*, vol. 35, no. 15, pp. 1212–1214, Jul. 1999.

[69] AWR Design Environment, a circuit simulator, version 9.02r, AWR Corporation, El Segundo, CA., USA. [Online]. Available: http://www.awrcorp.com (Cited Nov. 30, 2012).

[70] C.-H. Wu, K.-L. Wong, Y.-C. Lin, and S.-W. Su, ”Internal shorted monopole antenna for the watch-type wireless communication device for Bluetooth operation,” *Microwave and Optical Technology Letters*, vol. 49, no. 4, pp. 942–946, Apr. 2007.

[71] B. Lahey, A. Girouard, W. Burleson, and R. Vertegaal, ”PaperPhone: understanding the use of bend gestures in mobile devices with flexible electronic paper displays,” *The ACM CHI Conference on Human Factors in Computing Systems (CHI 2011)*, May 2011, Vancouver, BC, Canada, pp. 1303–1312.

[72] CTIA Test Plan for Mobile Station Over the Air Performance, Rev. 3.1, 410 p, Jan. 2011. [Online]. Available: http://files.ctia.org (Cited Nov. 30, 2012).

[73] C. Gabriel, ”Tissue equivalent material for hand phantoms,” *Physics in Medicine and Biology*, vol. 52., no. 14, pp. 4205–4210, 2007.

[74] T. M. Greiner, ”Hand anthropometry of U.S. army personnel,” Army Natick Research Development and Engineering Center, Technical Report Natick/TR-92/011, Dec. 1991.

[75] J. Holopainen, O. Kivekäs, J. Ilvonen, R. Valkonen, C. Icheln, and P. Vainikainen, ”Effect of the user’s hands on the operation of lower UHF-band mobile terminal antennas: focus on digital television receivers,” *IEEE Transactions on Electromagnetic Compatibility*, vol. 53, no. 3, pp. 831–841, Aug. 2011.

[76] J. Rahola and J. Ollikainen, ”Optimal antenna placement for mobile terminals using characteristic mode analysis,” *Proceedings of the 1st European Conference on Antennas and Propagation (EuCAP 2006)*, Nov. 2006, Nice, France.

Appendix A: Comparison of simulated and measured results

The reflection coefficients obtained using the different simulation software (SEMCAD, CST, HFSS) as well as with measurements using a VNA (Vector Network Analyser) are shown in the figures below. Altogether six different cases are considered, and also brief comments on the possible differences between simulation and measurement results are provided. All results are given for the case of unmatched antenna elements, which means that no matching circuit is applied.

In Figs. A.1–A.3, the comparison between simulations and measurements is shown in the case of the 105 mm ground plane. The curves of Fig. A.1 show that the general agreement between the measurements and the results given by the different simulation software is fairly good. In Fig. A.2, the agreement between simulations and SEMCAD is good up to 1.5 GHz, and above 1.8 GHz, the different simulation software provide very similar behaviour. The differences between the simulations may be caused by the slightly different simulation model, and in the measurement case, the properties of the materials around which the antennas are bent can cause some difference.

The measurement result of Fig. A.3 shows a standing wave above 1.3 GHz. The difference between simulated and measured results is most likely caused by the way in which the ground plane is bent. The copper sheet used is fairly rigid, meaning that obtaining a tight bending over the entire ground plane length is challenging (particularly challenging is the end in which the off-ground element is located). In the simulation models, the ground plane was bent along its entire length.

The curves of Figs. A.4–A.6 present the comparison between simulation and measurement results in the case of the 175 mm ground plane. In all three cases, the measured results have a slight offset towards higher frequencies above 1.5 GHz (resonant frequencies of the ground plane, general behaviour etc.). The offset is also present in the planar case, which means that the difference can be traced back to the measured prototype. Additional measurements performed for the planar case (see Fig. A.4) illustrate that the source of the difference is the location and tapping point of the coaxial feed cable.

With the 105 mm ground plane, the best location for the cable is known to be from

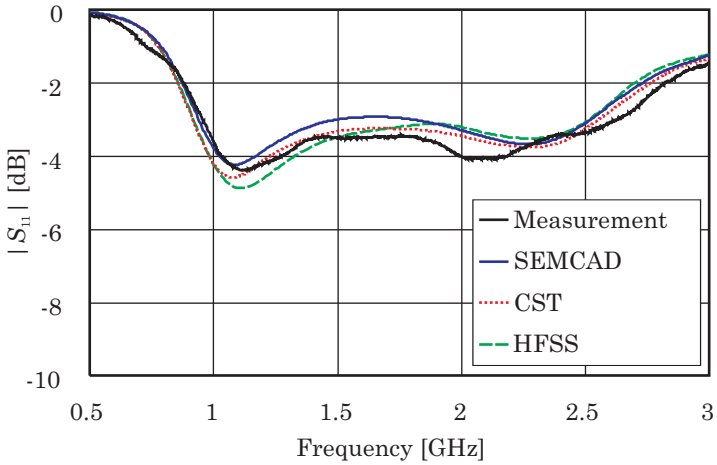

Fig. A.1. Comparison between measured and simulated $|S_{11}|$ for the 105 mm ground plane with no bending.

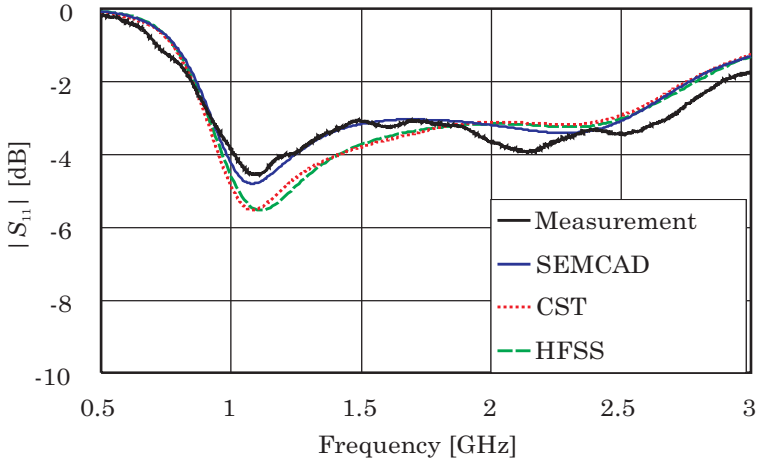

Fig. A.2. Comparison between measured and simulated $|S_{11}|$ for the 105 mm ground plane when 73.5 mm bending radius is applied.

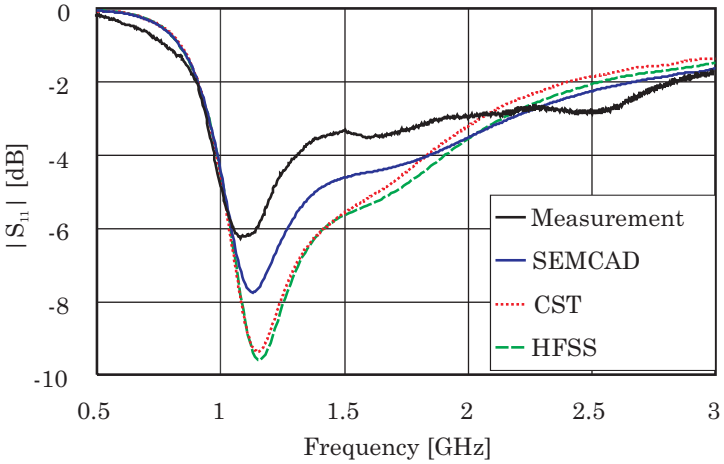

Fig. A.3. Comparison between measured and simulated $|S_{11}|$ for the 105 mm ground plane when 31.5 mm bending radius is applied.

the centre of the broad side of the ground plane, but the wavemodes of the 175 mm ground plane can be such that feeding cable should be brought to the ground plane

in a different way. The curves of Fig. A.4 show that by changing the positioning of the cable, the resonance seen in the simulations around 1.45 GHz can be observed. However, the general shape of the measured curves is in fairly good agreement with the simulated ones.

For both ground plane lengths, some ripple can be seen in the measured curves. The source of this uncertainty can be the cables and especially their connectors that experience quite a lot of strain and tension especially when the tightest bending cases are measured. In all measurements, a calibration cable (whose length equals that of the feeding cable of the prototypes) was used to obtain correct phase on the Smith chart at the feeding position for the measurements as compared with the simulations. The effect of the calibration cable cannot be seen in the Cartesian $|S_{11}|$ curves, though.

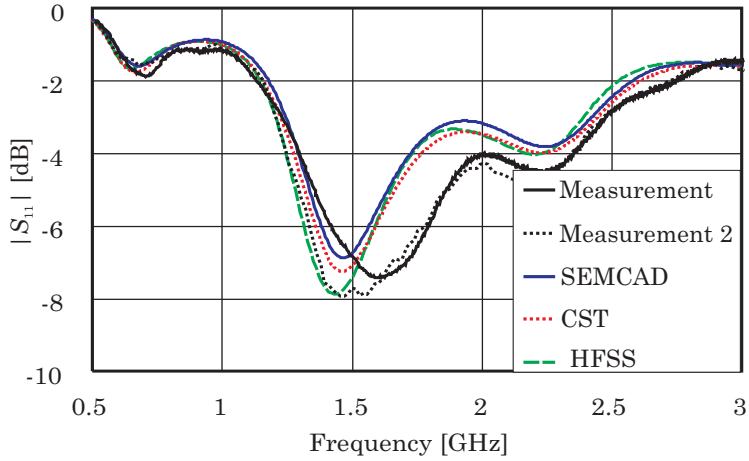

Fig. A.4. Comparison between measured and simulated $|S_{11}|$ for the 175 mm ground plane with no bending.

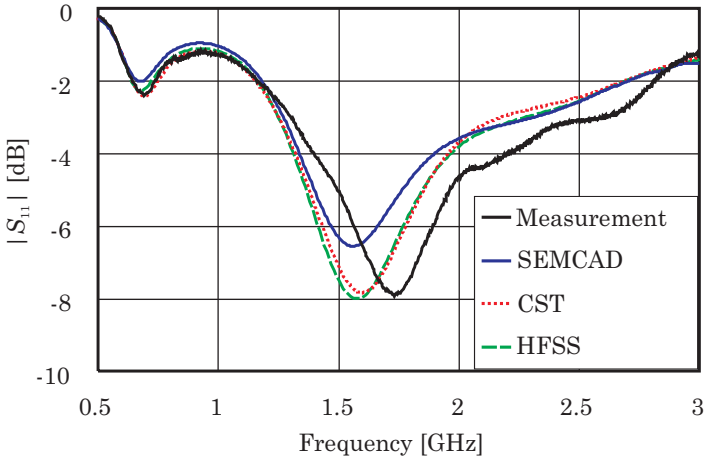

Fig. A.5. Comparison between measured and simulated $|S_{11}|$ for the 175 mm ground plane when 73.5 mm bending radius is applied.

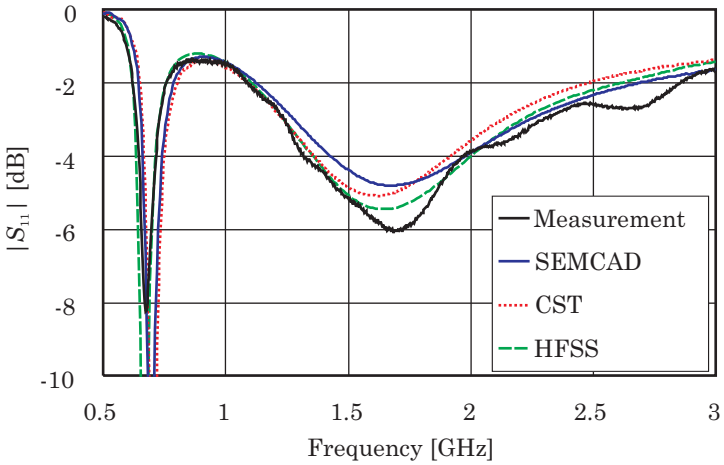

Fig. A.6. Comparison between measured and simulated $|S_{11}|$ for the 105 mm ground plane when 31.5 mm bending radius is applied.

Appendix B: Simulated unmatched reflection coefficients

The unmatched reflection coefficients obtained with the different bending radii for the two ground plane lengths and antenna cases studied are illustrated in this Appendix. The results show that as the bending radius increases, the unmatched reflection coefficient gradually converges to that of the planar, unbent case. The black dashed line in all of Figs. B.1–B.6 corresponds to the reflection coefficient of the planar case.

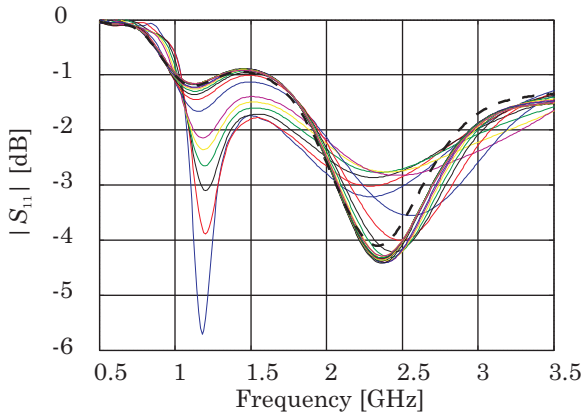

Fig. B.1. Unmatched reflection coefficient for CCE#1 (off-ground). Ground plane length is 105 mm.

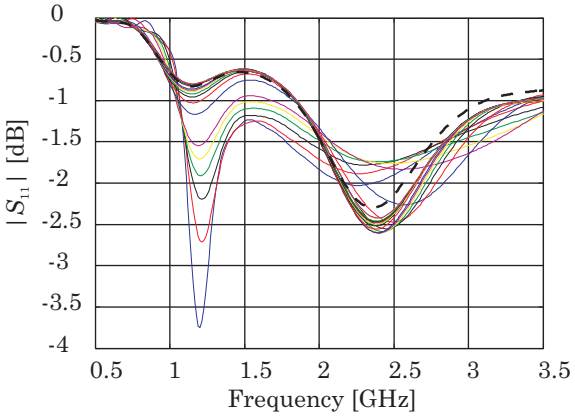

Fig. B.2. Unmatched reflection coefficient for CCE#1 (on-ground). Ground plane length is 105 mm.

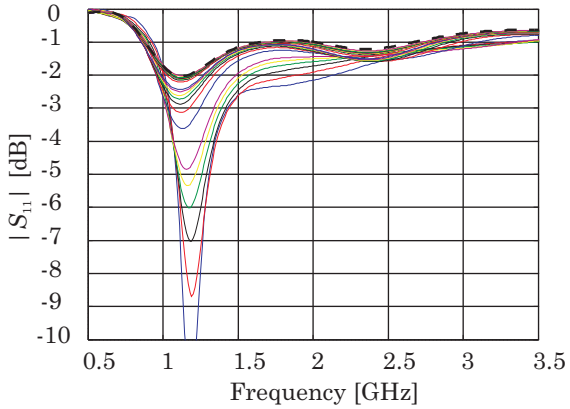

Fig. B.3. Unmatched reflection coefficient for CCE#1 (on-ground). Ground plane length is 105 mm.

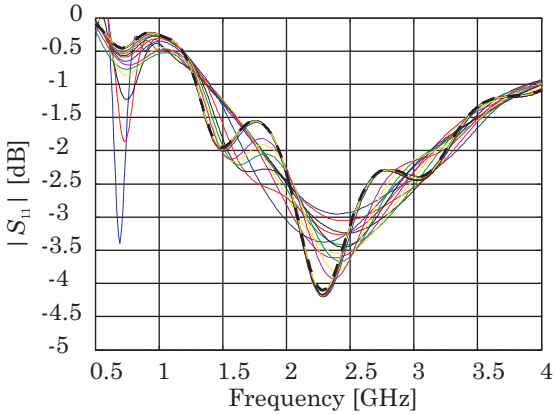

Fig. B.4. Unmatched reflection coefficient for CCE#1 (off-ground). Ground plane length is 175 mm.

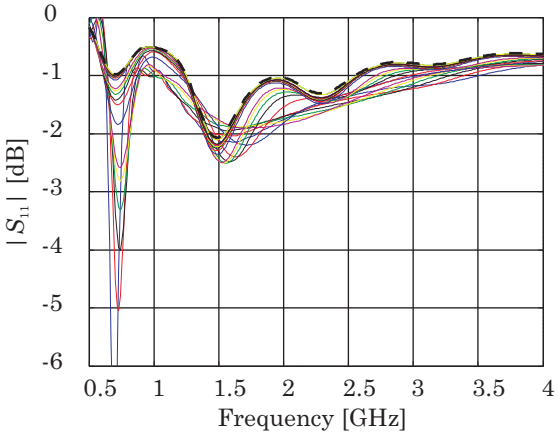

Fig. B.5. Unmatched reflection coefficient for CCE#1 (on-ground). Ground plane length is 175 mm.

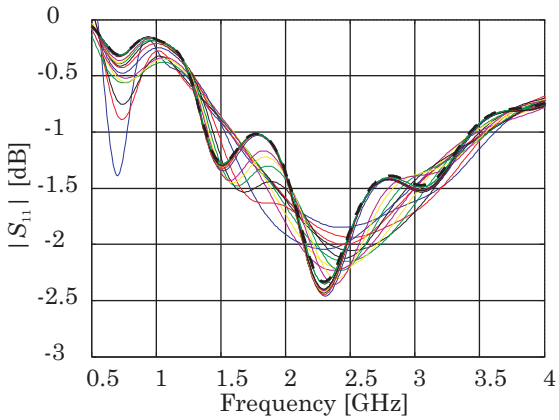

Fig. B.6. Unmatched reflection coefficient for CCE#1 (on-ground). Ground plane length is 175 mm.